X. PLASMAS AND CONTROLLED NUCLEAR FUSION

A. Active Plasma Systems*

Academic and Research Staff

Prof. A. Bers
Prof. G. D. Bernard
Prof. G. Bolz
Prof. W. D. Getty
Prof. J. G. Siambis
Prof. J. Taillet

Graduate Students

R. R. Bartsch
S. R. J. Brueck
J. A. Davis
F. N. Herba
B. R. Kusse
M. A. Lieberman
J. A. Mangano
R. R. Parker
R. D. Reilly
H. M. Schneider
R. N. Wallace

1. BEAM-PLASMA DISCHARGE: SYSTEM D

Microwave mode-shift electron density measurements have been made on System D for a beam-plasma discharge occurring in a side-injected gas pulse.[1] Two mode-shift techniques have been used: the shift of the TM_{010} mode of the discharge cavity at 740 Mc, and the higher order mode-shift technique of Fessenden.[2,3] Representative

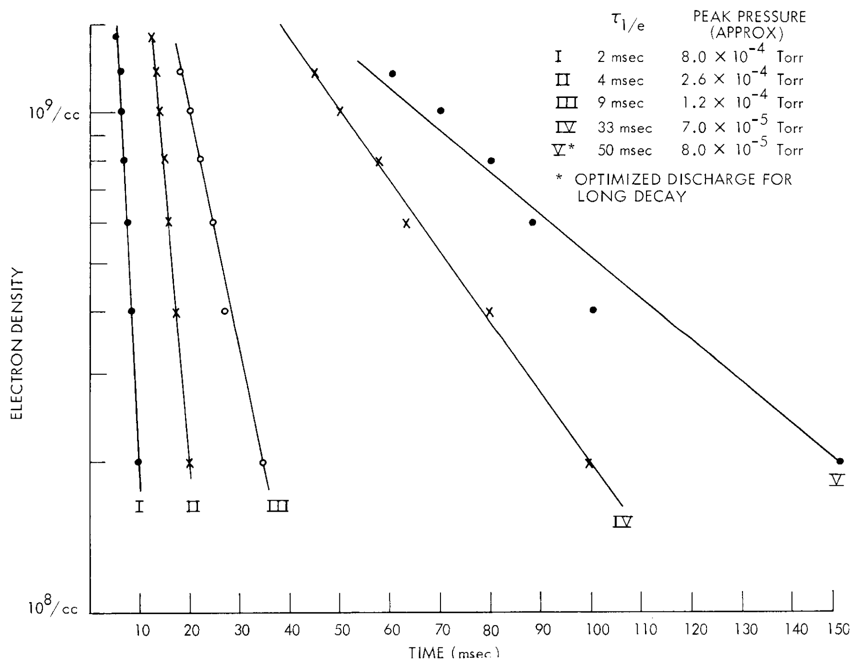

Fig. X-1. Fundamental mode-shift density decay measurement.

*This work was supported by the National Science Foundation (Grants GK-57 and GK-614).

density decays of the afterglow as measured by the shift of the fundamental mode are shown in Fig. X-1 for various peak pressures. The frequency shift of the TM_{010} mode is related to the electron density by the following expression, if we assume that the plasma density is $n = n_o \cos \pi\hat{x}/\ell\, J_o\,(2.405\, r/R_p)$ with cavity walls at $x = \pm L/2$ and the plasma radius, R_p, equal to half the discharge-tube radius (discharge tube radius = 13 cm).

$$n_o \text{ (in particles/cc)} = 10^2 \Delta f.$$

A typical electron density decay as measured by the higher order mode-shift technique is shown in Fig. X-2. The number of modes, ℓ, shifted past a given frequency

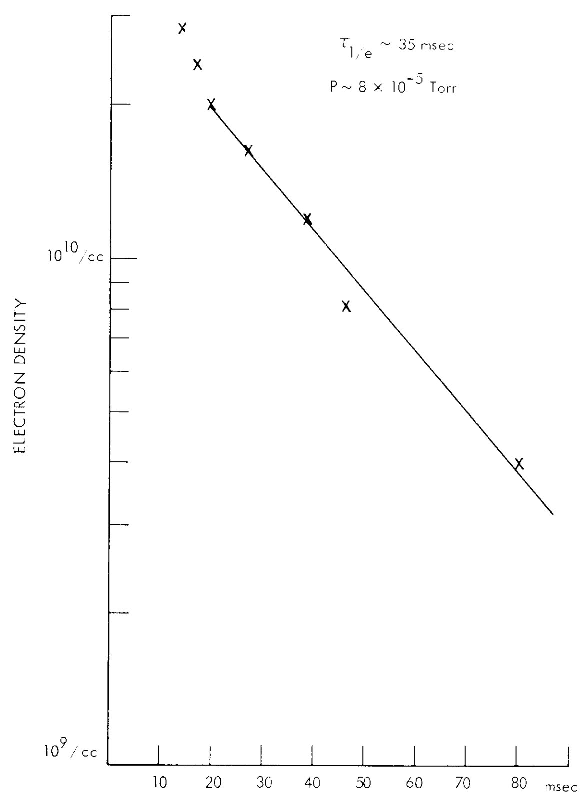

Fig. X-2. Higher order mode-shift electron density decay measurement.

is related to the mode spacing, δf, and the density as follows: n (in particles/cc) = $1300\, \ell \delta f$, where the frequency of operation is 10 kMc/sec. We expect the mode spacing at 10 kMc to be ≈200 kcps; however, the experimentally observed mode shift is 3 Mc/sec. The difference is due to the overlap of adjacent modes of the cavity. Only the modes that are strongly excited are detected as distinct modes.

No explanation has been found for the factor of 5 difference between the two density measurements. Data for each were taken on different runs, and the discharge with side injection is not always reproducible from pulse to pulse.

If we assume that the decay rate is governed by electron-neutral mirror scattering losses, then we may infer an electron energy for the hot-electron component of the plasma of approximately 5 keV, using the relations given in Quarterly Progress Report No. 80 (pages 128-132). Since the plasma diamagnetism (Fig. X-3) does not show an immediate drop after the electron beam pulse, we assume that the diamagnetism is caused by the hot electrons (the low-energy electrons will be lost from the system within a millisecond and we would expect the diamagnetism to fall just after the beam pulse to the level resulting only from the high-energy electrons).

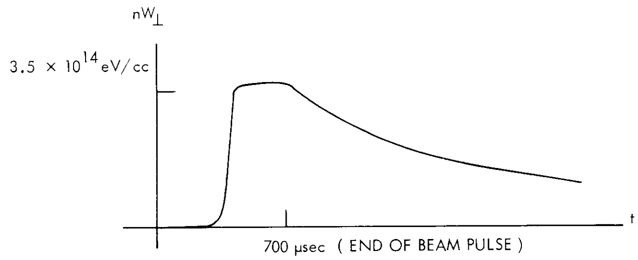

Fig. X-3. Transverse energy density from the diamagnetic signal.

The initial density of hot electrons is found to be $\approx 7 \times 10^{10}$/cc by dividing the initial diamagnetism by the energy per particle.

We can estimate the total electron density by assuming that cold electrons are produced and lost as follows: Ionizing collisions produce cold electrons at a rate given by

$$\nu_i = n_o \sigma_i v_e,$$

where n_o is the neutral (hydrogen) density, σ_i is the ionization cross section ($\sim 10^{-16}$ cm^2/ (E/.1 keV)$^{1/2}$), and v_e is the hot-electron velocity.[4] Cold electrons are lost from the system in the time that it takes a room-temperature ion to move half the length of the system (~1 msec). We have the following equation for the production and loss of cold electrons.

$$\frac{dn_c}{dt} + 10^3 n_c = 6 \times 10^{-8} n_o n_h(t),$$

where n_c is the density of cold electrons, n_h the density of hot electrons, and n_o the density of neutrals. If we assume that $n_o \approx 3 \times 10^{11}$/cc and the hot-electron decay is $7 \times 10^{10}\ e^{-\alpha t}$, where $\alpha^{-1} \gg 1$ msec, we have the following (neglecting the initial build-up transient) result:

$$n_c(t) = 1.3 \times 10^{12} e^{-\alpha t}\ \text{cm}^{-3}.$$

This analysis indicates that the density of cold electrons is approximately 20 times the density of hot electrons.

Further density measurements will be made with a Fabry-Perot interferometer and with a phase-shift interferometer to determine the density during the initial, high-density portion of the decay.[5] A Marshall valve is being constructed to give a faster, more reproducible gas pulse.[6]

The use of the facilities of the National Magnet Laboratory for this experiment is gratefully acknowledged.

R. R. Bartsch

References

1. L. D. Smullin, W. D. Getty, T. Musha, and R. R. Bartsch, Quarterly Progress Report No. 78, Research Laboratory of Electronics, M. I. T., July 15, 1965, pp. 102-105.
2. S. C. Brown and D. J. Rose et al., Technical Reports No. 66, 140, 222, 223, 230, Research Laboratory of Electronics, M. I. T.
3. T. J. Fessenden, Sc. D. Thesis, Department of Electrical Engineering, M. I. T., June 1965.
4. D. J. Rose and M. Clark, Jr., Plasmas and Controlled Fusion (The M. I. T. Press Cambridge, Mass., 1961), p. 39.
5. M. A. Lieberman, Quarterly Progress Report No. 76, Research Laboratory of Electronics, M. I. T., January 15, 1965, pp. 109-111.
6. H. Forsen, "Fast Acting Valve Which Operates at Temperatures up to 400°C," Rev. Sci. Instr. 35, 1362 (1964).

2. BEAM-PLASMA DISCHARGE: SYSTEM C

a. Digital Data System

In the course of experiments concerned with ion-cyclotron wave generation in System C, a need arose for a means of obtaining time-resolved averages of signals having relatively large variance. Standard methods of obtaining such averages (for example, sample-and-hold circuits followed by electronic integration) proved to be of little use, on account of the low repetition rate (1/sec). The difficulty was that the signal-to-noise ratio of a collection of samples ("signal" defined as mean, and "noise" as variance) improves as $\sqrt{N}$, where N is the number of samples. To obtain a reliable estimate of the mean, a large number of samples, say, 100, was required. Because of the low repetition rate, this involved a long real-time interval, and the long-term stability of existing circuitry was not sufficient to produce reliable results.

The problem was solved by using the digital system shown in Fig. X-4. The input signal is sampled at a given time with respect to the firing of the beam pulse. The sample is then converted to digital form by the analog-to-digital converter (ADC) and the digital form is counted and stored in a preselected channel of a 400-channel counter. The process is repeated once per beam pulse and each subsequent count is added to the count existing in the selected channel. When enough samples have been taken to insure

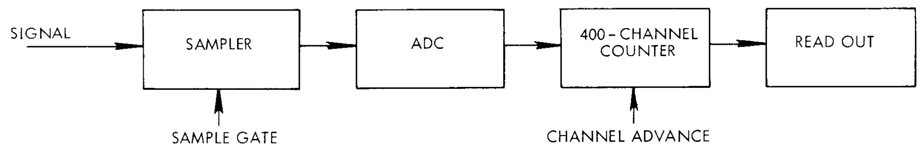

Fig. X-4. Digital data system.

reliability, the count is read out on a cathode-ray tube presentation or x-y recorder.

In the usual application, we want to obtain a plot of the sampled signal as a function of some variable such as magnetic field, distance into the discharge, and so forth. When this is the case, the variable is slowly changed by mechanical means and the counting channel is simultaneously advanced, again, only after a sufficient number of samples have been accumulated. If the variable is time relative to the initiation of the beam pulse, the time of the sampling gate may be slowly varied in the manner just described or, more efficiently, the "sample gate" may be a burst of 400 sampling gates uniformly distributed over the time of interest. In this mode it is necessary that each gate also serve as a channel advance, so that each sample is stored in a different channel, and that the whole system be reset before the occurrence of each beam pulse.

An example of the use of the system in the ion-cyclotron wave experiment[1] is shown in Fig. X-5. Here we have plotted the axial dependence of the azimuthal component of wave magnetic field as a function of distance from the collector for two frequencies.

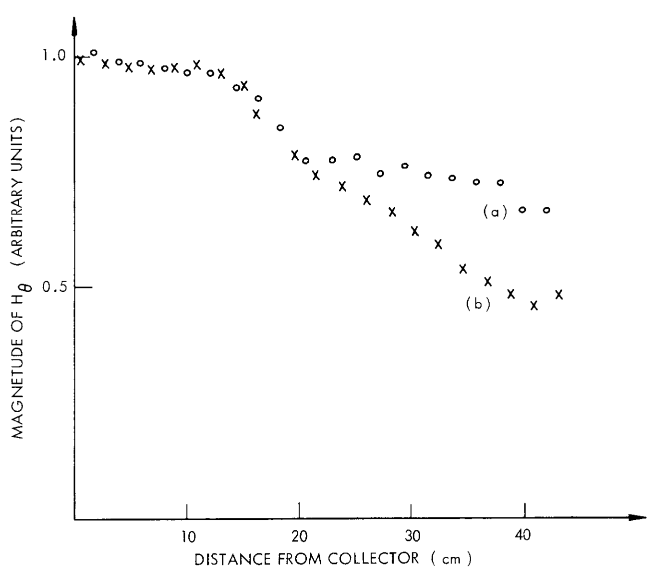

Fig. X-5. Plots of H_θ vs distance from collector: (a) f = 1.1 Mc; (b) f = 1.3 Mc with f_{ci} = 1.4 Mc.

Each point represents the average of approximately 50 pulses. Curves such as these are found to be very reproducible and are yielding valuable information on the propagation of waves near the ion-cyclotron frequency.

b. Ion-Cyclotron Wave Generation

We have previously reported effects associated with wave propagation in the plasma near ω_{ci}.[1] Further wave-field measurements, as well as measurement of the electrode impedance, have failed to reveal the expected rapid shortening of the wavelength for $\omega \lesssim \omega_{ci}$. This negative result must be a consequence of either damping processes that

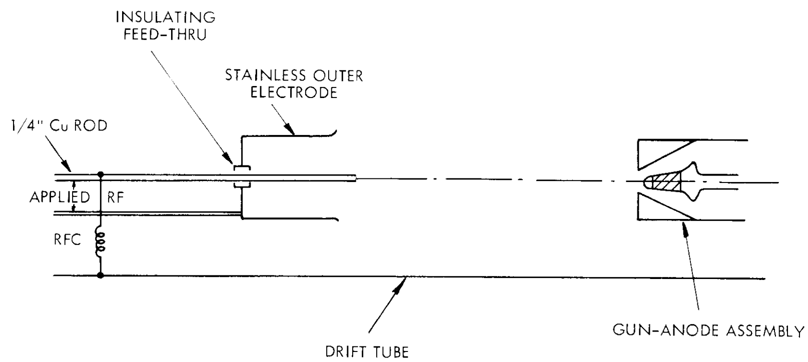

Fig. X-6. New wave-launching system.

are not contained within a theory based on cold plasma plus resistivity[2] or a larger resistivity than our experimental conditions predict.

To eliminate possible effects at the boundary of the plasma, we have installed the wave-launching system shown in Fig. X-6. The purpose of this system is to better confine the waves within the body of the plasma and thus minimize any effects associated with the plasma boundary. The first experiment was to measure the radial dependence of the azimuthal magnetic field at a point 45 cm from the beam collector and at a frequency of 1.06 Mc, well below the ion-cyclotron frequency of 1.4 Mc. The result is shown in Fig. X-7; thus our expectation that the wave fields are well contained within the plasma column is confirmed.

The curve shown in Fig. X-7 has an implication that may be important. From the cold-plasma plus resistivity theory one obtains a dispersion equation which, for the branch of interest, yields an axial wave number which, for $\omega < \omega_{ci}$, is essentially real and independent of radial wave number. (The last feature is a consequence of the small impedance presented to electron current flow along the field lines.) The implication, as far as the system of Fig. X-5 is concerned, is that the RF fields should be confined to an annular region defined by those field lines intersecting the outer surface of the inner electrode and the inner

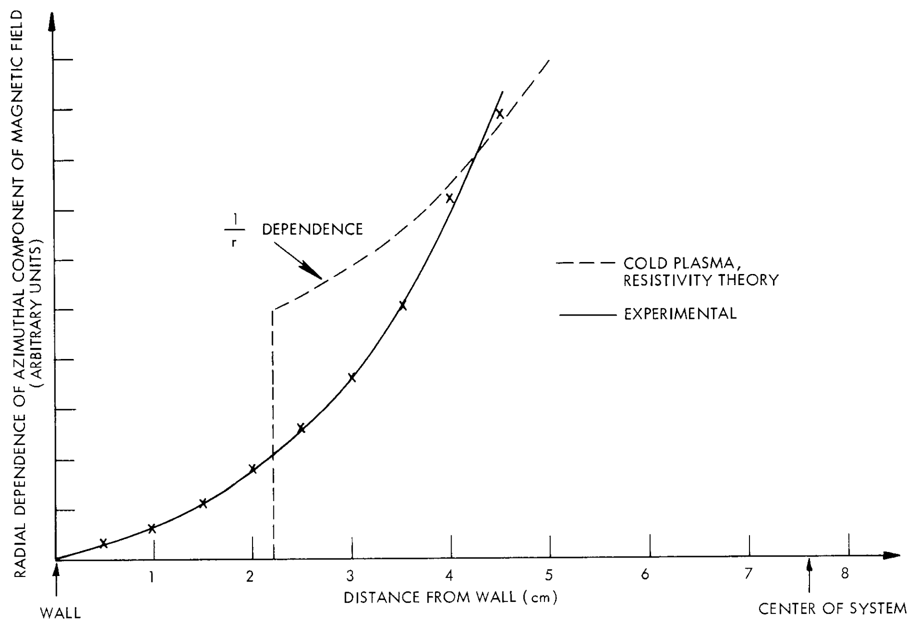

Fig. X-7. Radial dependence of wave field 45 cm from the collector, f = 1.06 Mc.

surface of the outer electrode. Hence, this theory predicts the radial dependence shown (dashed) on Fig. X-6. As this is not the case experimentally, we conclude that the cold-plasma plus resistivity theory does not adequately explain our results.

We are now considering the effects of viscosity on the cold-plasma theory, as well as the possibility of an enhanced resistivity resulting from the unstable nature of our beam-generated plasma. The last effect has apparently been observed in a hollow-cathode arc by Boulassier and co-workers, and many of our results could be explained simply as a result of an anomalously high resistivity.

R. R. Parker

References

1. R. R. Parker, "Beam-Plasma Discharge: System C," Quarterly Progress Report No. 80, Research Laboratory of Electronics, M.I.T., January 15, 1965, pp. 115-117.

2. F. I. Boley, J. M. Wilcox, A. W. DeSilva, P. R. Forman, G. W. Hamilton, C. N. Watson-Munro, "Hydromagnetic Wave Propagation near Ion Cyclotron Resonance," Phys. Fluids 6, 925 (1963).

3. J. C. Boulassier et al., Proc. VI Conference on Ionization Phenomena in Gases, Paris, 1963, Vol. I, p. 359.

3. ELECTRON BEAM EXCITATION OF ION OSCILLATIONS IN AN ECRD PLASMA

a. Beam-Excited Low-Frequency Oscillations

Strong electron beam-excited low-frequency oscillations (6-25 Mc) have been observed in the electron-cyclotron resonance discharge (ECRD). These oscillations appear over a wide range of discharge pressures, magnetic fields, and beam voltages. Typically, a 50-300 volt electron beam, of perveance 1×10^{-6}, is injected into a stainless-steel discharge tube, 7 inches in diameter and 3 ft long. Hydrogen gas is continuously admitted to the discharge tube so as to maintain a gas pressure of $1\text{-}10 \times 10^{-5}$ torr. A static magnetic field with a central value of 350-550 gauss and a mirror ratio of approximately 3 is maintained along the axis of the discharge tube. The ECRD is excited by a 2450-Mc "cooking" magnetron driven by an unfiltered, 3-phase power supply. RF power pulses approximately 2 msec long are generated every 8.3 msec, as shown in Fig. X-8. The average power incident on the ECRD plasma is 180 watts, while the absorbed power varies from 70 watts to 100 watts, over the range of pressures and magnetic fields encountered in this experiment.

When both the electron beam and the ECRD are simultaneously activated, strong low-frequency oscillations appear in the beam-collector current. These oscillations appear primarily in the afterglow region of the ECRD, as shown in the middle column of Fig. X-9. The oscillations disappear or are greatly reduced if either the beam or the plasma is turned off. Therefore they must arise from a beam-plasma interaction.

To study the axial variation of the beam-excited oscillations, a 4-ft section of 8-mm Pyrex glass tubing was sealed at one end and mounted against the discharge tube inner wall, with its length parallel to the axis of the discharge tube. A coaxial $\overline{\mathrm{E}}$ probe, 4 ft

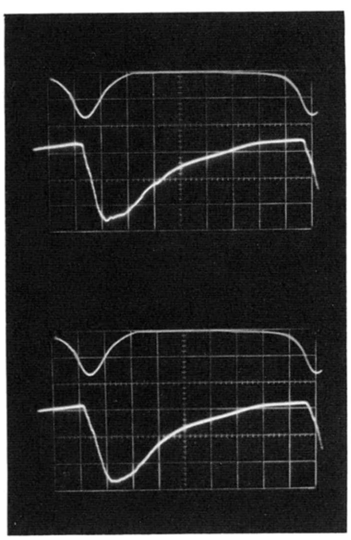

Fig. X-8.

RF power pulse and diamagnetic signal vs time. Upper trace: RF power pulse. Lower trace: diamagnetic signal. Time scale, 1.0 msec/cm.

long and 1/8 inch in diameter, was slid into the glass tube to study the variation of the axial electric field as a function of axial distance. Preliminary measurements indicate that the probe and glass tube do not disturb the beam or plasma, and that the

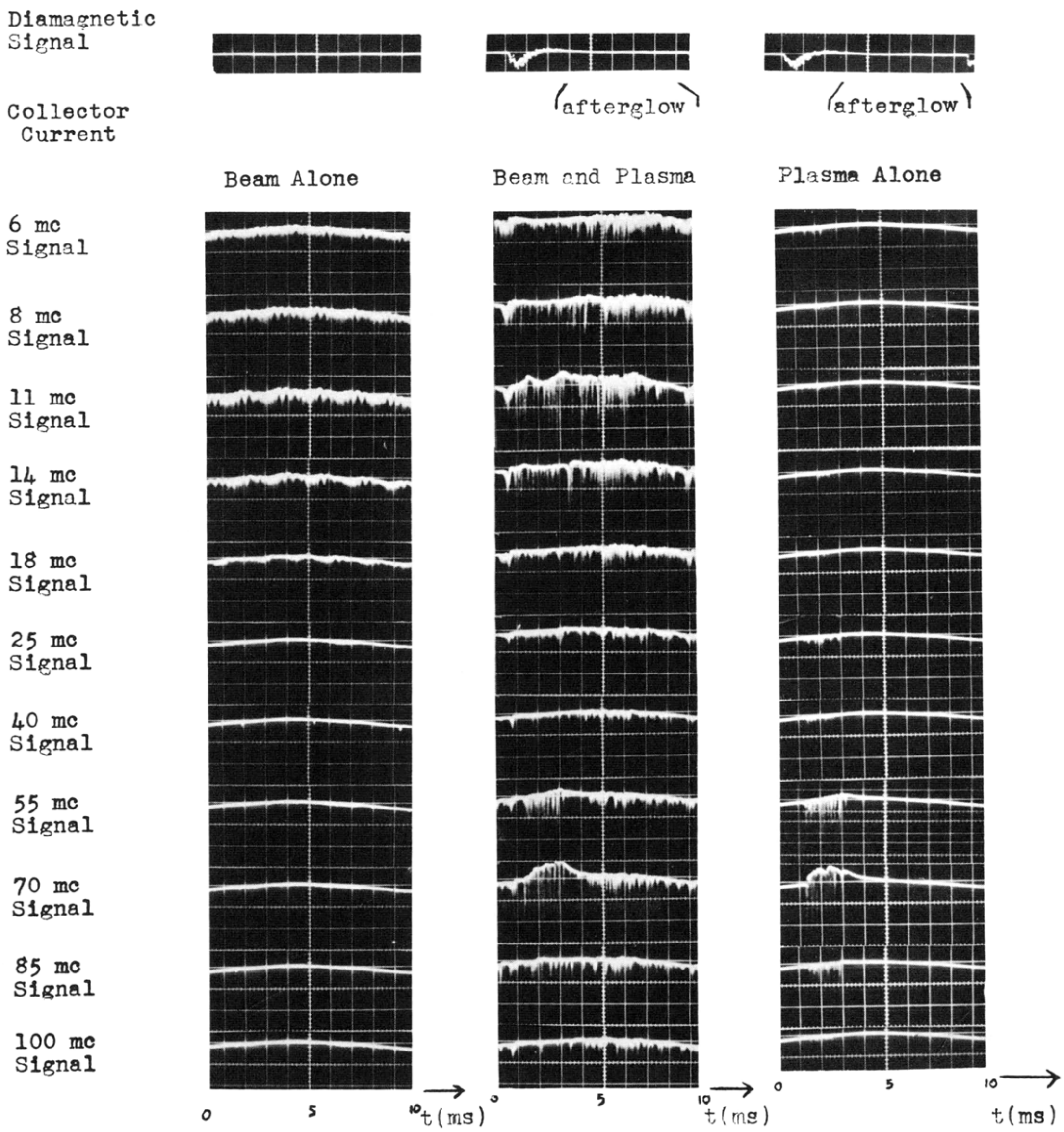

Fig. X-9. Time characteristics of the beam-excited RF oscillations. Pressure: 10^{-4} torr H_2 gas. Central magnetic field: 420 gauss. Average incident power: 180 watts. Average absorbed power: 80 watts. Beam voltage: 300 volts. Beam perveance: 1.0 microperve. Time scale: 1.0 msec/cm.

beam-excited oscillations observed in the collector current also appear on the axial probe. A rough sketch of the "strength" of the beam-excited oscillations as a function of axial distance is shown in Fig. X-10. This sketch shows that the oscillations are well confined to the center of the magnetic mirror. Since the E probe is against the inner discharge tube wall, the oscillations are not confined to the beam region in the center of the plasma, but extend outward radially to the discharge tube wall.

Previous attempts[1-4] with the same apparatus to observe a low-frequency beam-plasma interaction were unsuccessful. The electron beam was velocity-modulated at

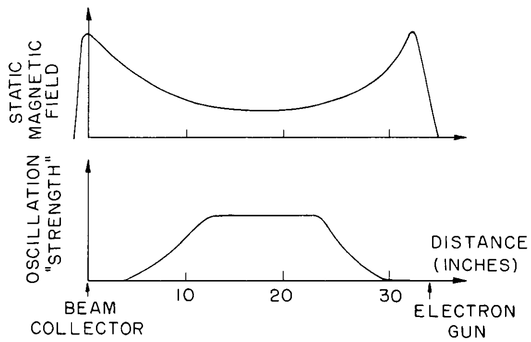

Fig. X-10.
Strength of the beam-excited RF oscillations as a function of axial distance.

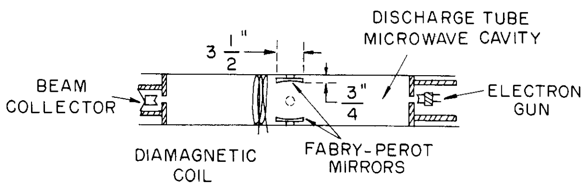

Fig. X-11.
Diagram of the discharge tube showing the Fabry-Perot mirrors and the diamagnetic coil. The RF power pulses are fed into the discharge tube through a circular port in the center of the tube.

low frequencies (20-200 Mc) in an effort to detect even a weak beam-plasma interaction, but no interaction was observed. The negative result of these experiments was traced to a pair of Fabry-Perot microwave interferometer mirrors which were placed inside the discharge tube to measure the plasma density. Each mirror was $3\frac{1}{2}$ inches in diameter and $\frac{1}{2}$ inch thick, and protruded approximately $\frac{3}{4}$ inch into the discharge tube, as shown in Fig. X-11. In the course of these experiments, a diamagnetic probe consisting of 40 turns of wire was wound around the discharge tube. With the Fabry-Perot mirrors in place, no diamagnetic signal could be observed. (Typical plasma densities of 10^9-10^{10} electrons/cm^3 were measured with the Fabry-Perot interferometer.) The mirrors were then removed, and a strong diamagnetic signal was detected. Simultaneously, the beam-excited low-frequency oscillations of Fig. X-9 made their appearance. If, with the mirrore absent, a glass or grounded metal rod is inserted in the radial direction more than $\frac{3}{4}$ inch into the discharge tube, then the diamagnetic signal is extinguished. It is unlikely that much plasma is present so close to the discharge tube wall. Wall sensors show that the plasma is well confined in the radial direction. More probably, the effect of the mirrors and radial rods is to modify the electric field in the discharge, so that the hot electrons are not contained by the mirror magnetic field. In any case, the Fabry-Perot mirrors were permanently removed from the system.

b. X-ray Bremsstrahlung Spectra

The ECRD generates a flux of x rays exceeding 5 roentgens/hr, for some values of the pressure and magnetic field. The Bremsstrahlung spectra of these x rays were measured by using a 400-channel pulse-height analyzer with a scintillating crystal of sodium iodide. The x-ray detector was collimated so that x rays generated at the walls of the discharge tube could not be detected by the scintillating crystal. Only x rays generated in the center of the magnetic mirror could pass through the collimator and reach the detector.

Time-resolved measurements of the x-ray spectra were made by gating the analyzer on for synchronized periods after each microwave power pulse. In this way, the time dependence of the spectra could be studied. A sypical time-resolved x-ray spectrum is shown in Fig. X-12. From the exponential falls of spectra such as these, the

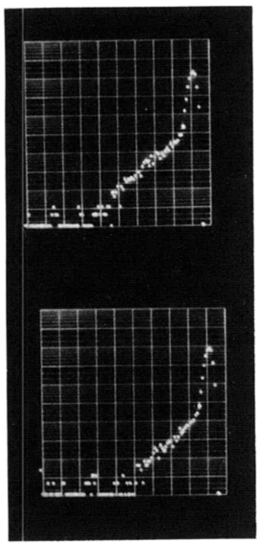

Fig. X-12. X-ray Bremsstrahlung spectrum. Ordinate: relative photon intensity on a logarithmic scale, 10^5 counts full scale. Abscissa: 75 keV full scale, reading from right to left. Central magnetic field: 420 gauss. Average incident power: 180 watts. Average absorbed power: 80 watts. Pressure: 2.7×10^{-4} torr H_2 gas. Analyzer gated on for 1.0 msec, beginning 2.0 msec after the initial rise of the diamagnetic signal.

"temperature" of the hot electrons was determined. If the electron distribution is Maxwellian, then the Bremsstrahlung spectrum should fall[5] as exp (-E/T), where T is the temperature of the electrons (in energy units) and $\overline{E}$ is the photon energy.

Experimental studies of the x-ray spectra for various magnetic fields and pressures have yielded the following results:

(i) The "tail" of the electron distribution function is Maxwellian, corresponding to a "temperature" of 5-9 keV.

(ii) The "temperature" as a function of time is roughly constant. The only effect of looking at longer times after each power pulse is a decrease in the photon intensity; thus a decay of the plasma density is indicated. The exponential fall of the x-ray spectrum remains constant.

It is possible to calculate a decay time τ_s for the hot-electron component of the plasma. The hot-electron density decays because the hot electrons are scattered into the loss cone of the magnetic mirror and lost. The dominant scattering process in the

ECRD is electron-neutral collisions. For scattering of fast electrons by neutrals, the scattering frequency[6] is

$$\frac{1}{\tau_s} = \frac{p}{T^{3/2}} 3.1 \times 10^7 (1+.275 \ln T), \tag{1}$$

where p is the neutral gas pressure in torr, and T is the electron energy in kilovolts.

The decay time τ_s calculated from (1) can be compared with the decay of the diamagnetic signal. Figure X-8 shows a typical diamagnetic signal during one power pulse of the ECRD. This signal is obtained by integrating the voltage developed across a 40-turn coil wrapped around the outside of the discharge tube. After the RF power pulse has ended, the diamagnetic signal decays exponentially with a time constant τ_D. In Table X-1, τ_D and τ_s are compared for various pressures.

Table X-1. Scattering times τ_s and τ_d for various pressures. Average magnetic field: 420 gauss. Average incident power: 180 watts. Average absorbed power: 80 watts.

Pressure (torr)	τ_s (msec)	τ_D (msec)
1.9×10^{-4}	1.4	1.8
2.6×10^{-4}	1.9	1.9
5.2×10^{-4}	0.8	1.0

In calculating τ_s, the neutral-gas pressure was measured with a Bayard-Alpert gauge, which was calibrated against a McLeod gauge to give a measurement of absolute pressure. The hot-electron "temperature" was determined by the x-ray Bremsstrahlung measurements.

M. A. Lieberman, A. Bers

References

1. Quarterly Progress Report No. 73, Research Laboratory of Electronics, M.I.T., April 15, 1964, pp. 81-85.
2. Quarterly Progress Report No. 75, Research Laboratory of Electronics, M.I.T., October 15, 1964, pp. 120-121.
3. Quarterly Progress Report No. 76, Research Laboratory of Electronics, M.I.T., January 15, 1965, pp. 109-111.
4. Quarterly Progress Report No. 77, Research Laboratory of Electronics, M.I.T., April 15, 1965, pp. 137-140.
5. T. J. Fessenden, Sc.D. Thesis, Department of Electrical Engineering, M.I.T., June 1965, p. 117.
6. Ibid., p. 105.

4. INSTABILITIES IN HOT-ELECTRON BEAM-PLASMA SYSTEMS

In a hot-electron, Maxwellian plasma, the dispersion function $D(\omega, k, \ldots)$ is transcendental, and no analytical method for obtaining its roots exists. Therefore, computer solutions are often necessary. A computer program to find the roots of D has been written. This program uses the Newton-Raphson method to follow a root of D as some parameter of the dispersion function D is varied. The user must provide an initial guess that is "close" to the root he wishes to follow. Using this program, the dispersion diagrams of several beam-plasma systems have been studied.

a. Longitudinal Waves in a Cold-Ion Hot-Electron Plasma

In Quarterly Progress Report No. 79 (pages 126-130) the dispersion equation for longitudinal waves in a cold-ion, hot-electron plasma was considered:

$$1 - \frac{\omega_{pi}^2}{\omega^2} - \frac{\omega_{pb}^2}{(\omega-\beta V_o)^2} + \frac{1}{\beta^2\lambda_D^2}\left[1 + \frac{1}{\sqrt{2}\,\beta\lambda_D}\frac{\omega}{\omega_{pe}} Z\left(\frac{1}{\sqrt{2}\,\beta\lambda_D}\frac{\omega}{\omega_{pe}}\right)\right] = 0. \tag{1}$$

The discussion of this dispersion equation given there must be corrected. The caption on p. 129 of Q.P.R. No. 79 should read: (a) $\eta = \frac{1}{4}$ (b) $\eta = 1$ where $\eta = \frac{n_b}{n_p}\frac{V_T^2}{V_o^2}$. Thus Briggs' condition[1] $\eta > 1$ for a strong ion interaction is not met for either of the dispersion diagrams in Quarterly Progress Report No. 79 (page 129). In fact, as Briggs has pointed out,[2] the condition $\eta > 1$ leads to an ion interaction in a Maxwellian plasma in which the gain is infinite for frequencies just below ω_{pi}. Thus, one always has a solution of Eq. 1 with $|\beta| \to \infty$ as $\omega \to \omega_{pi}$. A stability analysis shows that this solution is evanescent for $\eta < 1$ and convectively unstable for $\eta > 1$.

Figure X-13a shows the dispersion diagram of the convectively unstable solution of Eq. 1 for $\eta < 1$. The stability analysis for this solution is presented in Fig. X-13b. The gain is finite and is peaked at a frequency slightly below ω_{pi}. For $\omega < \omega_{pi}$, the gain is large and represents reactive medium amplification of the slow beam wave by the "inductive" plasma ions. For $\omega > \omega_{pi}$, the gain is very small and represents resistive medium amplification of the slow beam wave by the Landau damped plasma electrons.

Figure X-13c shows the transition occurring when $\eta > 1$. The convectively unstable solution of Eq. 1 now has an infinite growth rate for ω slightly below ω_{pi}. The stability analysis for this solution is shown in Fig. X-13d.

The gain mechanism is a reactive medium amplification for $\omega < \omega_{pi}$ and resistive (Landau damping) medium amplification for $\omega > \omega_{pi}$, as before. Note that in the weak-beam limit $n_b \ll n_p$, the condition $\eta = 1$ requires $V_T \gg V_o$. Landau damping is small in

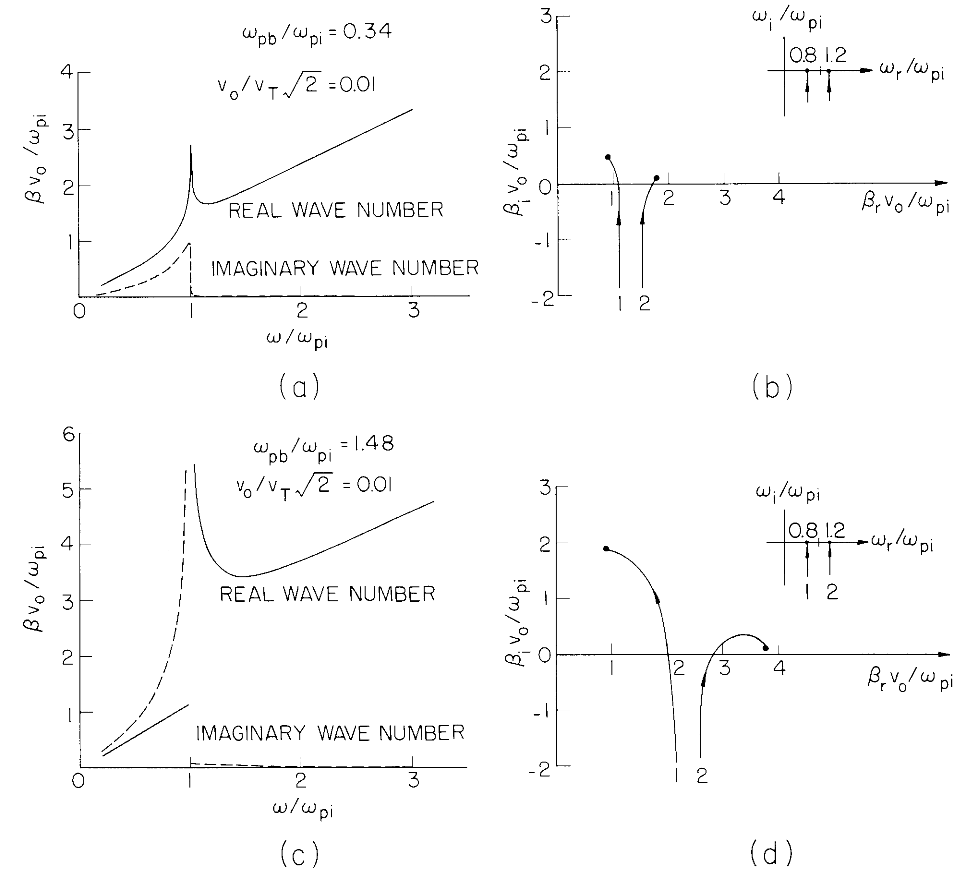

Fig. X-13. Beam-plasma dispersion equation for longitudinal waves (Landau damping and ion motions included). (a) η = 0.32. (b) Stability criteria for η = 0.32. (c) η = 6.0. (d) Stability criteria for η = 6.0.

this limit, so the resistive medium amplification rates are very small.

It is clear from Eq. 1 that a finite ion temperature would lead to a finite growth rate at ω_{pi} in all cases.

b. Onset of the Absolute Ion Instability in a Hot-Electron, Beam-Plasma Waveguide

Consider a waveguide of radius a whose axis is parallel to the static magnetic field $\overline{B}_o$. The waveguide is uniformly filled with a plasma consisting of cold ions and Maxwellian electrons of thermal velocity V_T. An electron beam uniformly filling the waveguide drifts along the magnetic fluid with a constant velocity V_o.

Under the assumption that as a boundary condition the tangential electric field vanishes at the walls, the quasi-static dispersion equation is

$$K_e + K_i + K_b - 2 = 0, \tag{2}$$

where

$$K_i = 1 - \frac{k_\parallel^2}{k^2}\frac{\omega_{pi}^2}{\omega^2} - \frac{k_\perp^2}{k^2}\frac{\omega_{pi}^2}{\omega^2 - \omega_{ci}^2} \tag{3}$$

$$K_b = 1 - \frac{k_\parallel^2}{k^2}\frac{\omega_{pb}^2}{(\omega - k_\parallel V_o)^2} - \frac{k_\perp^2}{k^2}\frac{\omega_{pb}^2}{(\omega - k_\parallel V_o)^2 - \omega_{ce}^2} \tag{4}$$

$$K_e = 1 + \frac{\omega_{pe}^2}{k^2 V_T^2}\left[1 + \sum_{n=-\infty}^{\infty} I_n(\lambda)\, e^{-\lambda}\, \zeta_o Z(\zeta_n)\right] \tag{5}$$

$$\lambda = \frac{k_\perp^2 V_T^2}{\omega_{ce}^2} = \left(\frac{\text{Larmor radius}}{\text{Waveguide radius}}\right)^2 \tag{6}$$

$$\zeta_n = \frac{\omega - n\omega_{ce}}{k_\parallel V_T \sqrt{2}} \tag{7}$$

and the linearized potential is assumed to vary as

$$\exp[-j(\omega t - k_\parallel z)]\, J_m(k_\perp r)\, e^{jm\phi}. \tag{8}$$

The boundary condition at the waveguide wall requires that

$$k_\perp = \frac{\epsilon_{m\ell}}{a}, \tag{9}$$

where $\epsilon_{m\ell}$ is the ℓ^{th} zero of J_m. Consider the limit of large magnetic fields, for which $\lambda \ll 1$ and $\omega_{pb} \ll \omega_{ce}$, but $\omega_{pi} \gg \omega_{ci}$. For many beam-plasma systems of interest, these assumptions are well satisfied. Physically, they state that the beam and plasma electrons are constrained to move only along the field lines. The transverse motion of the ions is allowed, however, because of their larger mass. Excluding cyclotron harmonic frequencies $n\omega_{ce}$ and wave numbers for which $k \approx \omega_{ce}/V_o$, the dispersion equation (2) can be written

$$k_\parallel^2\left[1 - \frac{\omega_{pi}^2}{\omega^2} - \frac{\omega_{pb}^2}{(\omega - k_\parallel V_o)^2} - \frac{\omega_{pe}^2}{2k_\parallel^2 V_T^2} Z'\left(\frac{\omega}{k_\parallel V_T \sqrt{2}}\right)\right] + k_\perp^2\left[1 - \frac{\omega_{pi}^2}{\omega^2 - \omega_{ci}^2}\right] = 0, \tag{10}$$

where Z' is the derivative of the plasma dispersion function, tabulated by Fried and Conte.[3]

Several authors have studied Eq. 10 under one approximation or another. Briggs[1] considered the limit $\omega/k_{\|}V_T\sqrt{2} \ll 1$ and showed that an absolute instability could exist near the ion plasma frequency ω_{pi}, even when the plasma in the absence of the beam supports only a forward travelling wave. This result cannot be predicted by weak coupling theory. Briggs' condition for the absolute ion instability can be written

$$\omega_{pb} \gtrsim \omega_{pi}, \qquad \text{provided } V_T/V_o \gg 1. \tag{11}$$

Puri[4] and Wallace[5] both considered a dispersion equation similar to (10), in which the hot electrons were represented by a rectangular velocity distribution function instead of a Maxwellian. Their condition for the absolute ion instability can be written

$$\omega_{pb} \gtrsim \omega_{pi}, \quad V_T \gtrsim V_o. \tag{12}$$

Both Puri and Wallace realized that their condition (12), obtained for a rectangular distribution of electrons, could not be applied to a Maxwellian distribution in the region of heavy Landau damping $V_T \sim V_o$. Therefore, their condition (12) does not correctly describe the onset of the absolute ion instability in a Maxwellian plasma. This condition can be obtained only by properly accounting for the Landau damping.

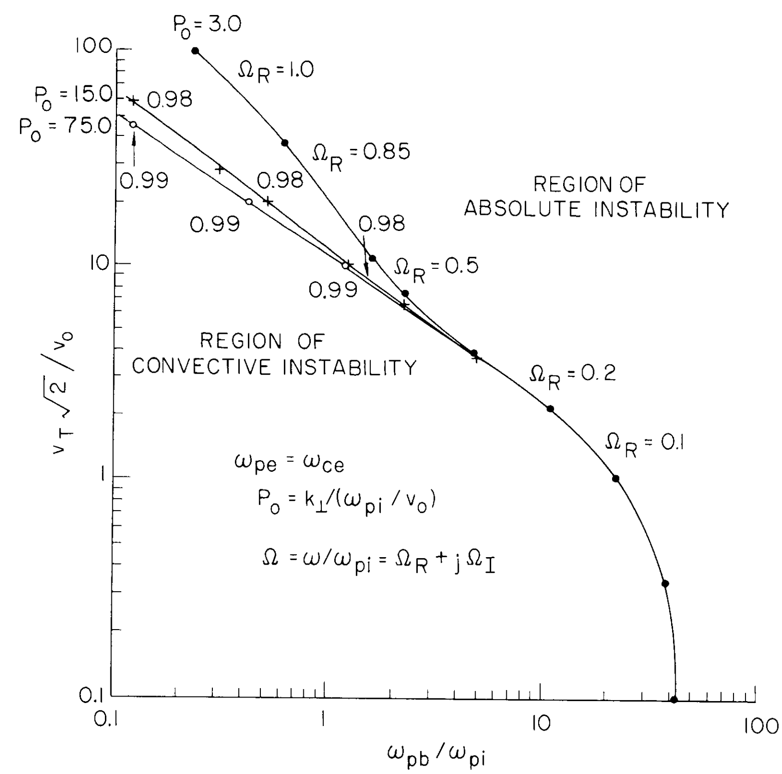

Fig. X-14. Onset of absolute ion instability in a hot-electron beam-plasma waveguide.

In this report the condition for the onset of the absolute ion instability in a Maxwellian plasma has been determined by numerically setting the ℓhs of (10) and its derivative with respect to $k_{\parallel}$ equal to zero. For a given set of system parameters, the frequency ω and wave number $k_{\parallel}$ are determined from these two equations. The additional constraint Im $\omega = 0$ then imposes a relation among the system parameters, which is the onset condition. This condition is shown in Fig. X-14. The quantity $V_T\sqrt{2}/V_o$ is plotted along the ordinate, and the quantity ω_{pb}/ω_{pi} is plotted along the abscissa. For a given value of $P_o = k_{\perp}V_o/\omega_{pi}$, the onset condition Im $\omega = 0$ divides the graph into two regions. In the upper right-hand region, the absolute ion instability is obtained. In the lower left-hand region, only a convective instability exists. Alongside the line Im $\omega = 0$, and for each value of P_o, the real part of the normalized frequency ω/ω_{pi} is specified. This frequency is the oscillation frequency of the beam-plasma system at the onset of absolute instability.

The onset condition has been computed for $\omega_{ce} = \omega_{pe}$ as pertinent to our beam-plasma experiment in an ECRD plasma. The magnetic field $\overline{B}_o$ enters into the problem only through the ion cyclotron frequency ω_{ci}, so, for $|\omega| \gg \omega_{ci}$, the onset condition Im $\omega = 0$ is essentially independent of the magnetic field.

M. A. Lieberman, A. Bers

References

1. R. J. Briggs, Electron Stream Interaction with Plasmas (The M.I.T. Press, Cambridge, Mass., 1964), Chapter 5.
2. R. J. Briggs, Private communication (1966).
3. B. Fried and S. Conte, The Plasma Dispersion Function (Academic Press, New York, 1961).
4. S. Puri, "Electron Beam Interaction with Ions in a Warm Electron Plasma," S.M. Thesis, Department of Electrical Engineering, M.I.T., June 1964. See also Quarterly Progress Report No. 74, pp. 121-128.
5. R. N. Wallace, "An Investigation of Complex Waves in Electron Beam-Plasma Systems," S.M. Thesis, Department of Electrical Engineering, M.I.T., September 1964. See also Quarterly Progress Report No. 76, pp. 111-117.

5. THEORY OF VHF OSCILLATIONS AND POSSIBLE INTERACTIONS WITH IONS IN THE BEAM-PLASMA DISCHARGE

In the beam-plasma discharge, a pulsed electron beam of moderate perveance when injected into a low-pressure gas produces a plasma to which it gives up a considerable portion of its DC kinetic energy. In his study of the beam-plasma discharge, Getty[1] observed strong RF oscillations and scattering of beam electrons across confining magnetic fields of several hundred gauss. Hsieh[2] studied the frequency spectrum and time dependence of the RF power radiated by the beam-plasma discharge in some detail. He observed RF radiation principally in two bands of frequencies, the kMc band (7 kMc to 27 kMc) and the VHF band (30 Mc to 600 Mc). Hsieh interpreted the kMc oscillations as electron plasma oscillations. This interpretation was verified by Getty, who actually measured the density of the plasma. In experiments with different gases, Hsieh attempted to interpret the VHF oscillations as ion plasma oscillations; however, the results of these experiments were inconclusive.

It is shown here that the gross features of the frequency spectrum of the VHF oscillations observed in the beam-plasma discharge may possibly be understood in terms of a model in which the VHF oscillations arise from the interaction of a filamentary electron beam with a uniformly filled cold-plasma waveguide immersed in a uniform, longitudinal magnetic field. This interaction causes a snaking or "firehose" motion of the beam, corresponding to an azimuthal wave number n equal to plus or minus one. Since the gain for this interaction is relatively small and the interaction is convective, an efficient feedback mechanism is a necessary part of this model.

In the model, the kMc oscillations are electron plasma oscillations; that is, the oscillations are characteristic of the electron plasma frequency ω_{pe}. The VHF oscillations are not "tied" to the ion plasma frequency ω_{pi}, but rather arise from the coupling between a propagating plasma wave and a slow-beam cyclotron wave. The frequency at which this coupling occurs may turn out to be in the vicinity of ω_{pi}.

a. Experimental Observations of the Beam-Plasma Discharge by Hsieh

Figure X-15 illustrates the time characteristics of the beam generated plasma studied by Hsieh, in which a 200-μsec pulse of electron beam current is injected into a volume of gas at pressures of 10^{-3}-10^{-4} torr in a magnetic mirror to produce a plasma. The idealized plasma geometry of the beam-plasma discharge is shown in Fig. X-16.

At some time T_B (≈ 50 μsec) into the beam pulse, a burst of strong oscillations near ω_{ce} (≈ 800 Mc) appears. These oscillations are accompanied by scattering of beam electrons across the confining magnetic field and by a rapid rise in the plasma density. These oscillations near ω_{ce} usher in the regime of beam-plasma discharge proper. This regime is characterized by steady light and diamagnetic signals, by energetic plasma electrons (as evidenced by the X-ray signal) and by strong RF oscillations. The frequency spectra of these RF oscillations were measured by Hsieh for three different time intervals within the beam-plasma discharge and for three different gases. The behavior of these frequency spectra can be summarized as follows:

(i) The RF radiation is concentrated in two bands of frequencies, the kMc band (7-27 kMc) and the VHF band (30-600 Mc).

(ii) There is a missing band of frequencies, extending from 600 Mc to 7 kMc <u>and</u>

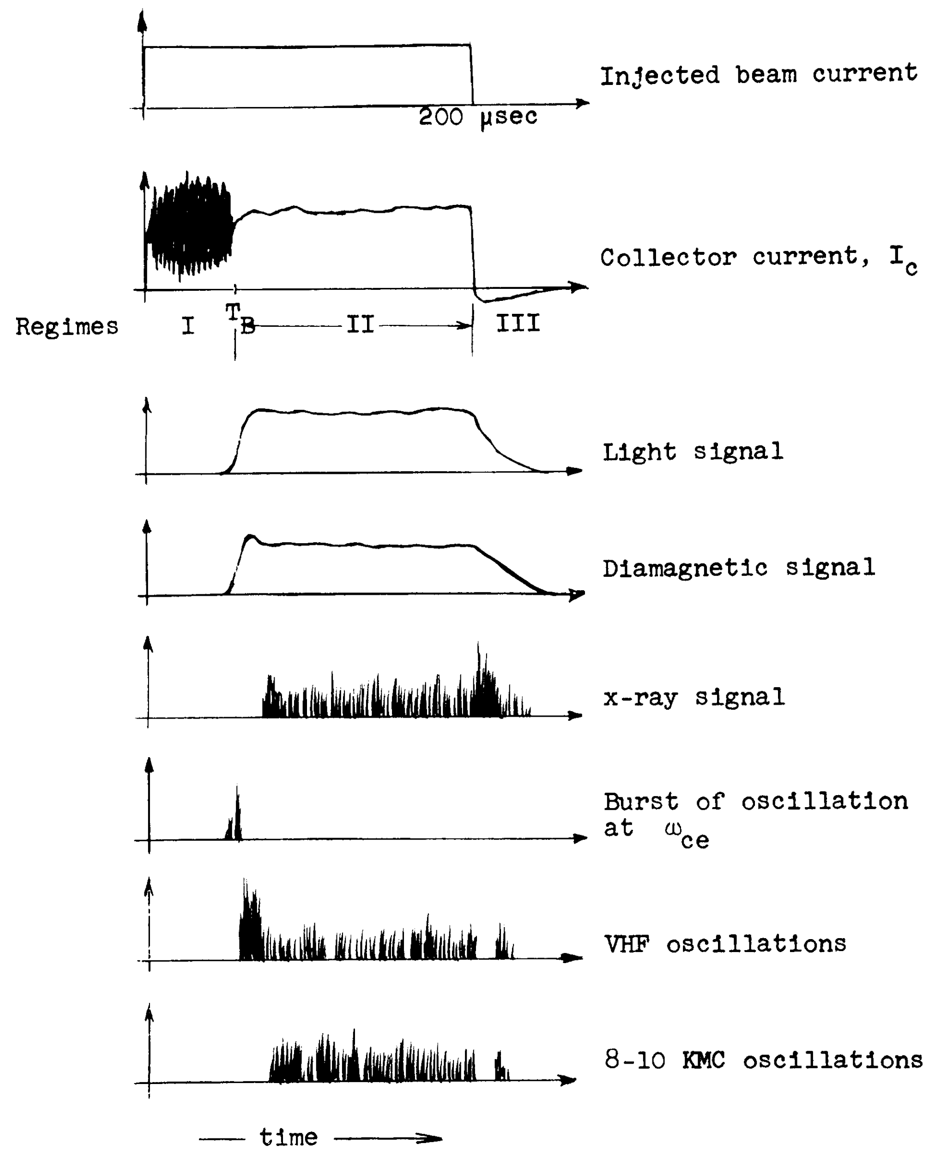

Fig. X-15. Time characteristics of the beam-plasma discharge (after H. Hsieh, Sc. D. Thesis, M.I.T., 1964, p. 37).

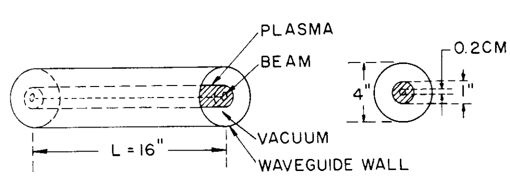

Fig. X-16. Idealized plasma geometry of the beam-plasma discharge (after H. Hsieh, Sc.D. Thesis, M.I.T., 1964).

including the electron cyclotron frequency ω_{ce} (890 Mc), in which no RF oscillations are observed.

(iii) The kMc band shifts toward higher frequencies as the delay time, the beam voltage or the gas pressure is increased.

(iv) The frequency spectrum of the VHF oscillations is relatively independent of the delay time, type of gas, gas pressure, and (over a limited range) beam voltage.

b. Weak Coupling of a Filamentary Electron Beam with a Cold Plasma Waveguide

Physically, the VHF oscillations can be understood in terms of two dispersion diagrams, Figs. X-17 and X-18. These two dispersion diagrams show the coupling of beam and plasma waves for the circularly symmetric (azimuthal wave number $n = 0$, Fig. X-17) and noncircularly symmetric ($n = \pm 1, \pm 2$, etc., Fig. X-18) modes in the filamentary beam approximation.

The model is a plasma-filled waveguide of radius a. An electron beam of radius $b \ll a$ flows down the center of the waveguide. The electrons and ions of the plasma have zero temperature. Experimentally, the VHF oscillations are observed for frequencies roughly one-half to one-third of the electron cyclotron frequency ω_{ce}. For such frequencies, the filamentary beam approximation can be made and proved to be valid. This approximation stated that

$$\begin{aligned} pb &\ll 1 \\ qb &\ll 1, \end{aligned} \tag{1}$$

where p and q are the transverse wave numbers in the beam and plasma regions, respectively. In this approximation, only two beam waves appear for the $n = 0$ mode (n is the azimuthal wave number, $n = 0$ is the circularly symmetric mode). These waves are the "beam space-charge" waves. No "beam cyclotron" waves appear for the $n = 0$ mode. This is to be expected, since the electric field is purely longitudinal at the position of the beam ($r = 0$) for this mode.

A synchronism between the "slow beam-space-charge" wave and the propagating plasma wave can only occur if the beam velocity v_o is equal to the phase velocity v_{ph} of a plasma wave somewhere in the VHF region.

In Fig. X-17 we show the situation generally occurring in the beam-plasma discharge for the $n = 0$ mode. The phase velocity v_{ph} of the forward propagating plasma waves in the VHF region is less than or equal to $\frac{\omega_{ce}}{x_{nm}} a$, where x_{nm} is the n^{th} zero of the m^{th}-order Bessel function J_m. Since in the beam-plasma discharge

$$v_o > \frac{\omega_{ce} a}{x_{oo}} > \frac{\omega_{ce} a}{x_{no}} > v_{ph}, \tag{2}$$

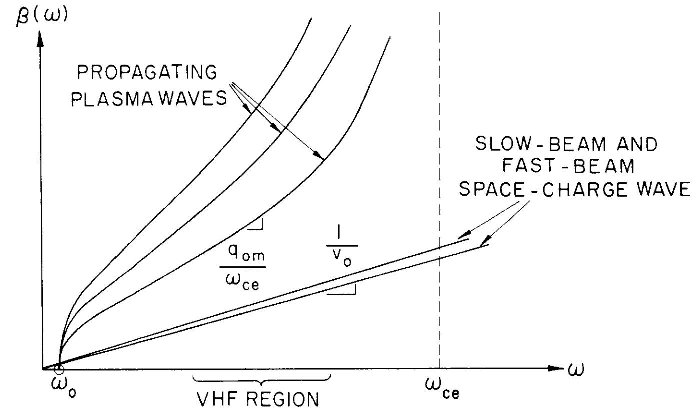

Fig. X-17. Beam waves and propagating plasma waves for the n = 0 (circularly symmetric) mode.

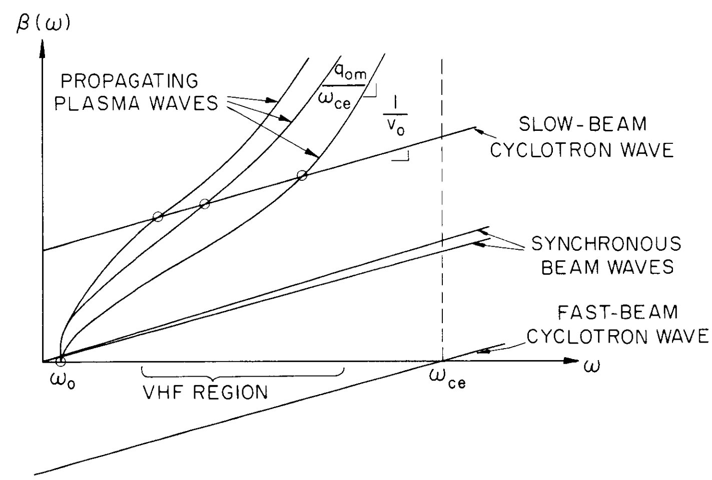

Fig. X-18. Beam waves and propagating plasma waves for the n ≠ 0 (noncircularly symmetric) modes.

no intersection occurs in the VHF region. The intersection in Fig. X-17 near the lower hybrid frequency $\omega_o = \frac{1}{43}\,\omega_{ce}$ is not within the VHF region.

In Fig. X-18, the situation generally occurring in the beam-plasma discharge is shown for all modes other than the n = 0 mode. The n = ±1 modes are the "fire-hose" modes, corresponding to a snaking motion of the beam. The n = ±2 modes have a double angular variation, and so on. For each pair (±1, ±2, ±3, etc.) of noncircularly symmetric modes, four beam waves appear: two "synchronous" beam waves and two "cyclotron" beam waves. The slow cyclotron wave intersects the plasma waves in the VHF region, as shown by the circles in Fig. X-18. This intersection between a negative and positive energy wave must lead to a convective instability.

The dispersion equation for the interaction of a filamentary beam with a cold plasma waveguide is[3,4]

$$\frac{\omega_{pb}^2}{\omega_d(\omega_d+\omega_{ce})} = \frac{2K_\perp}{1+\frac{\pi}{4}q^2b^2\frac{N_1(qa)}{J_1(qa)}}. \tag{3}$$

Near synchronism between the slow-beam cyclotron wave and the propagating plasma waves of Fig. X-18, $J_1(qa) \approx 0$. Expanding J_1 in a Taylor series, one finds

$$J_1(qa) \approx -\frac{2}{\pi\beta_o N_1(q_{n1}a)}(\beta-\beta_o). \tag{4}$$

Using (4), one can cast (3) into the form

$$(\beta-\beta_o)\left(\beta-\frac{\omega}{v_o}-\frac{\omega_{ce}}{2v_o}-\frac{1}{v_o}\sqrt{\frac{\omega_{ce}^2}{4}+\frac{\omega_{pb}^2}{2K_\perp}}\right) = -c_o^2(\omega). \tag{5}$$

Here, $c_o(\omega)$ is to be evaluated at the synchronous frequency and is given by

$$c_o(\omega) = \frac{\pi\omega_{pb}q_{n1}bN_1}{4v_o}\left(\frac{\omega}{2K_\perp}\right)^{\frac{1}{2}}\left(\frac{\omega_{ce}^2}{4}+\frac{\omega_{pb}^2}{2K_\perp}\right)^{\frac{1}{4}}. \tag{6}$$

The maximum amplification rate occurs exactly at synchronism and is

$$(\beta_i)_{max} = c_o(\omega). \tag{7}$$

c. Comparison Between Theory and Experiment

The theoretical growth rates have been calculated from Eq. 7. For the experimental parameters shown in tabular form below, the first few interaction frequencies and their growth rates are

$\omega_1 = 460$ mc $\qquad \beta_{i1} = .0048$/cm

$\omega_2 = 380$ mc $\qquad \beta_{i2} = .0054$/cm

$\omega_3 = 240$ mc $\qquad \beta_{i3} = .0052$/cm

These growth rates are quite small. The effect of a finite temperature or collision frequency on the magnitude of these gains has not been investigated.

These amplification rates could not by themselves lead to the observed VHF oscillations. For a 40-cm system, these rates correspond to a power amplification of only 1.6 db over the length of the discharge. Unless the power is fed back to the entering beam, oscillations at these frequencies will not take place. Therefore, a feedback mechanism is a necessary part of this theory if it is to be relevant for explaining the observed VHF oscillations in the beam-plasma discharge. One possible feedback device is the plasma wave propagating in the negative z direction. This wave has a negative real β and a negative group velocity v_g. It is the mirror image (about the frequency axis) of the forward propagating plasma wave shown in Fig. X-18. This negative z-directed wave is only slightly perturbed by the filamentary beam. The feedback system then consists of the positive z-directed wave having a gain $\approx .005$/cm and a group velocity v_o, coupled with the negative z-directed wave having a gain of unity and a group velocity v_g. Oscillations will build up in this feedback system at a rate ω_i given by

$$\omega_i = \beta_i \frac{v_o v_g}{v_o + v_g}. \tag{8}$$

For the parameters of Table X-1, the time constant $\tau = 2\pi/\omega_i$ for the buildup of VHF oscillations in the discharge is

$$\tau = 1\ \mu\text{sec}. \tag{9}$$

Thus this simple feedback mechanism might explain the observation of VHF oscillations in the beam-plasma discharge.

A detailed study of the predictions of the filamentary beam theory shows:

1. In the frequency range 460 Mc < f < 2.7 kMc, which includes the cyclotron frequency f_{ce} = 890 Mc, no RF oscillations should be present.

2. Below 460 Mc, VHF oscillations should be excited which display a mode structure; that is, the frequency spectrum of these oscillations should consist of a series of peaks which begin to blur together as the frequency f is decreased greatly below 460 Mc.

3. The RF intensity of the VHF oscillations should be greater near the beginning of the beam-plasma discharge since the amplification rate β_i given by (7) is a monotonically decreasing function of plasma density.

4. The VHF oscillation frequencies should be only a function of ω_{ce}, v_o, and a. That is, the frequencies at which VHF oscillations occur should be independent of the plasma density, type of gas, gas pressure, beam perveance, beam diameter, and beam density. On the other hand, the oscillation amplitudes should be functions of all these parameters.

These theoretical predictions are all borne out by Hsieh's data.

Table X-1. Typical parameters for the beam-plasma discharge studied by Hsieh.

Beam pulse length = 170 μsec
Beam breakup T_B = 4 to 6 μsec
Beam voltage V_b = 6 kev
  Beam velocity $v_o = 4.6 \times 10^9$ cm/sec
Beam perveance $K = 1.0 \times 10^{-6}$
Beam diameter 2b = 0.2 cm
  Beam density $n_b = 2.0 \times 10^{10}$ cm^{-3}
  Beam-plasma frequency ω_{pb} = 1.3 kMc = 8.0×10^9/sec
Mirror ratio $R \approx 3$
Central magnetic field B_o = 280 gauss
  Electron cyclotron frequency ω_{ce} = 0.89 kMc = 5.6×10^9/sec
  Ion cyclotron frequency ω_{ci} = 0.48 Mc = 3.0×10^6/sec H_2
  Hybrid frequency $\sqrt{\omega_{ce}\omega_{ci}}$ = 21.0 Mc = 1.3×10^8/sec H_2
Plasma diameter 2a = 2.5 cm
Pressures: 1.1×10^{-3} torr H_2
  2.8×10^{-3} torr He
  2.5×10^{-4} torr A
Electron plasma frequency ω_{pe} = 15 to 25 kMc (94-156 $\times 10^9$/sec)
  Plasma density n_p = 3.5 to 4.5 $\times 10^{12}$ cm^{-3}

d. Small-Signal Ion and Electron Energies

One can calculate the small signal electron and ion oscillation energies for the VHF oscillations occurring in the beam-plasma discharge. This calculation is independent of the particular mechanism which drives the oscillations. One assumes only that VHF oscillations exist and that they are oscillations of a cold electron-ion plasma immersed in a static magnetic field $\overline{B}_o$.

Using the small-signal ion and electron force equations and assuming plane wave propagation at an angle to the magnetic field, one finds that the ratio of the ion-to-electron oscillation energy is given by

$$E_i/E_e = \frac{m}{M} \frac{1 + \omega^2 \left|\frac{K_{\parallel}}{K_{\perp}}\right| \frac{\omega^2 + \omega_{ci}^2}{\left(\omega^2 - \omega_{ci}^2\right)^2}}{1 + \omega^2 \left|\frac{K_{\parallel}}{K_{\perp}}\right| \frac{\omega^2 + \omega_{ce}^2}{\left(\omega^2 - \omega_{ce}^2\right)^2}}, \tag{10}$$

where $K_{\|}$ and $K_{\perp}$ are the parallel and perpendicular dielectric constants of the plasma. For VHF frequencies $\left(\omega \sim \frac{\omega_{ce}}{3}\right)$, $E_i/E_e \approx 2\frac{m}{M}$. Therefore the VHF oscillations do not represent ion motions. No significant amount of ion oscillation energy exists at VHF frequencies.

e. Suggestions for Beam Interactions with Ions in a Cold Plasma

The ratio E_i/E_e is unity at the lower hybrid frequency $\omega_o = \sqrt{\omega_{ce}\omega_{ci}}$. The ratio E_i/E_e continues to rise as the frequency is decreased, and has a resonance at the ion cyclotron frequency ω_{ci}. The detection of RF oscillations in this frequency range in the beam-plasma discharge would indicate the presence of significant ion motions.

If energy is to be transferred from an electron beam directly to the ions of a plasma, two conditions must be satisfied.

1. There must be an interaction frequency ω for which unstable waves exist in the beam-plasma system.

2. The ratio E_i/E_e of ion-to-electron oscillation energies must be reasonably large at this interaction frequency.

There are two interaction frequencies that satisfy both of these conditions in a cold-plasma waveguide: the ion cyclotron frequency ω_{ci} and the lower hybrid frequency $\omega_o = \sqrt{\omega_{ce}\omega_{ci}}$. The growth rates for beam-plasma interactions near the ion cyclotron frequency ω_{ci} are usually quite small. One is thus led to consider whether a beam-plasma interaction at the lower hybrid frequency ω_o could significantly excite ion motions.

Convective instability at the lower hybrid frequency ω_o arises from two mechanisms:

1. reactive medium amplification for frequencies slightly below ω_o.

2. synchronous interaction between a slow beam space-charge wave and a propagating plasma wave, for frequencies slightly above ω_o.

The growth rates at the hybrid frequency ω_o can be quite large. For example, in the filamentary beam approximation, reactive medium amplification rates[3,4] of 0.06/cm are obtained in the beam-plasma discharge. "Ion heating" might thus be accomplished by modulating the electron beam at the lower hybrid frequency ω_o.

M. A. Lieberman, A. Bers

References

1. W. D. Getty, Sc.D. Thesis, Department of Electrical Engineering, M.I.T., February, 1962.
2. H. Y. Hsieh, Sc.D. Thesis, Department of Electrical Engineering, M.I.T., June, 1964.
3. M. A. Lieberman, "Theory of VHF Oscillations in the Beam-Plasma Discharge," Internal Memorandum No. 1, December, 1965 (unpublished).
4. R. J. Briggs, Electron-Stream Interaction with Plasmas (The M.I.T. Press, Cambridge, Mass., 1960), Section 4.2.2. The notation is that of Briggs.

6. QUASI-LINEAR THEORY OF NARROW-BANDWIDTH CONVECTIVE INSTABILITIES

Consider an electron beam that is injected into a semi-infinite electron-ion plasma, plasma waveguide or other slow-wave structure. For many beam-plasma systems, linearized theory predicts that the interaction between beam and plasma gives rise to a narrow-bandwidth, convective instability.[1] By a convective instability, one means that the linearized fields vary as

$$\exp[j(\omega t-\bar{\beta}\cdot\bar{r})],$$

where the frequency ω is taken to be purely real, and $\bar{\beta}$ is complex. The imaginary part of β describes the growth or decay in space of the waves arising from the beam-plasma interaction. In many systems, these spatially growing waves are narrow-bandwidth; that is, the gain $\bar{\beta}_i(\omega)$ is sharply peaked within a small frequency region $\Delta\omega \ll \omega_o$ about the frequency of maximum gain ω_o. The dispersion diagram for narrow-bandwidth, convective instability is shown in Fig. X-19.

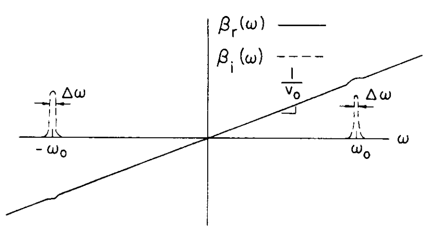

Fig. X-19. Dispersion of a narrow-bandwidth, convective instability.

In this report, we would like to investigate the onset of nonlinear effects and obtain a description of the slowing down of the electron beam. The theory and computations presented in a previous report[2] were found to be largely erroneous.

a. Formulation of the Quasi-Linear Theory

Each of the N species (beam electrons, plasma electrons, plasma ions, etc.) is described by the collisionless Vlasov equation

$$\left[\frac{\partial}{\partial t}+\bar{v}\cdot\frac{\partial}{\partial\bar{r}}+\frac{e}{m}(\bar{E}+\bar{v}\times\bar{B})\cdot\frac{\partial}{\partial\bar{v}}\right]f_i = 0. \tag{1}$$

These N equations are coupled through a curl-free electric field $\bar{E}$ (we make the electrostatic approximation):

$$\frac{\partial}{\partial\bar{r}}\times\bar{E} = 0 \tag{2}$$

$$\epsilon_o\frac{\partial}{\partial\bar{r}}\cdot\bar{E} = \sum_i e_i n_i \int f_i\, d\bar{v}. \tag{3}$$

A time average $\langle\ \rangle$ can be defined:

$$\langle\ \rangle \equiv \frac{1}{T_o} \int_0^{T_o} dt, \tag{4}$$

where

$$\frac{2\pi}{\omega_o} \ll T_o \ll \frac{2\pi}{\Delta\omega}. \tag{5}$$

Since the gain is narrow-bandwidth, the averaging time T_o always exists.

Let us define two functions

$$f_o(\bar{r}, \bar{v}, t) \equiv \langle f(\bar{r}, \bar{v}, t) \rangle \tag{6}$$

$$f_1(\bar{r}, \bar{v}, t) \equiv f(\bar{r}, \bar{v}, t) - f_o(\bar{r}, \bar{v}, t). \tag{7}$$

It follows immediately that

$$\langle f_1 \rangle = 0. \tag{8}$$

Thus f has been decomposed into the sum of a slowly varying and a rapidly varying function of time.

We assume that no external electric field is applied, from which

$$\langle E \rangle = 0. \tag{9}$$

We then write

$$\overline{E}(\bar{r}, t) = 0 + \overline{E}_1(\bar{r}, t). \tag{10}$$

Substituting (7) and (10) in the Vlasov equation (1) yields

$$\left[\frac{\partial}{\partial t} + \bar{v}\cdot\frac{\partial}{\partial \bar{r}} + \frac{e}{m}\left(\overline{E}_1 + \bar{v}\times\overline{B}_o\right)\cdot\frac{\partial}{\partial \bar{v}}\right](f_o+f_1) = 0. \tag{11}$$

Time averaging (11), we get

$$\left(\frac{\partial}{\partial t} + \bar{v}\cdot\frac{\partial}{\partial \bar{r}} + \frac{e}{m}\bar{v}\times\overline{B}_o\cdot\frac{\partial}{\partial \bar{v}}\right) f_o = -\frac{e}{m}\frac{\partial}{\partial \bar{v}}\cdot\langle \overline{E}_1 f_1 \rangle. \tag{12}$$

Subtracting (12) from (11) yields

$$\left(\frac{\partial}{\partial t} + \bar{v}\cdot\frac{\partial}{\partial \bar{r}} + \frac{e}{m}\bar{v}\times\overline{B}_o\cdot\frac{\partial}{\partial \bar{v}}\right) f_1 + \frac{e}{m}\overline{E}_1\cdot\frac{\partial f_o}{\partial \bar{v}} = -\frac{e}{m}\frac{\partial}{\partial \bar{v}}\cdot\left\{\overline{E}_1 f_1 - \langle \overline{E}_1 f_1 \rangle\right\}. \tag{13}$$

Note that if $\overline{E}_1$ and f_1 are first-order quantities in some small parameter, then the right-hand sides of both (12) and (13) are second-order in this parameter. This suggests an iterative scheme for solving (12) and (13), in which the right-hand sides of both equations are initially set to zero. One then recovers the equations of linearized theory.

In the procedure of quasi-linear theory,[3] the right-hand side of (13) alone is set equal to zero. The solutions f_1 and E_1 of Eq. 13 are then explicitly obtained in terms of the unknown function f_o. When these solutions are substituted in the right-hand side of (12), a nonlinear differential equation for f_o is obtained. It is the fundamental equation of quasi-linear theory:

$$\left(\frac{\partial}{\partial t}+\bar{v}\cdot\frac{\partial}{\partial\bar{r}}+\frac{e}{m}\,\bar{v}\times\bar{B}_o\cdot\frac{\partial}{\partial\bar{v}}\right)f_o=-\frac{e}{m}\frac{\partial}{\partial\bar{v}}\cdot\langle\bar{E}_1(f_o)f_1(f_o)\rangle. \tag{14a}$$

One can show that if the wave vector $\bar{\beta}$ is independent of f_o, then the product E_1f_1 appearing in (14a) would be a linear function of f_o. In this case (14a) reduces to a diffusion equation:

$$\frac{\partial}{\partial t}+\bar{v}\cdot\frac{\partial}{\partial\bar{r}}+\frac{\partial}{\partial\bar{v}}\cdot\left(\bar{\bar{D}}(\bar{r},\bar{v})\cdot\frac{\partial f_o}{\partial\bar{v}}\right)=0, \tag{14b}$$

where $\bar{\bar{D}}(\bar{r},\bar{v})$ is the diffusion tensor.

In the interest of mathematical tractability, (14a) will be linearized by setting the wave vector $\bar{\beta}$ equal to its initial value when the beam first enters the interaction region. One expects this linearization to be valid, provided the diffusion of the beam does not significantly alter the value of the gain $\beta_i(\omega)$ from its initial value. Provided the gain is limited by other factors (finite transverse boundaries, finite plasma temperature, etc.), the effect of beam diffusion on the wave vector $\bar{\beta}(\omega)$ should be unimportant during the initial stage of the interaction.

b. Diffusion Coefficient in One Dimension

We consider a one-dimensional problem and derive the diffusion coefficient D. Let us assume that the electron beam can be described by the one-dimensional Vlasov equation

$$\left(\frac{\partial}{\partial t}+v\frac{\partial}{\partial z}+\frac{e}{m}\bar{E}\cdot\frac{\partial}{\partial v}\right)f(z,v,t)=0. \tag{15}$$

The linearized solutions (E_1, f_1) are given by

$$\bar{E}_1=-\frac{\partial\Phi_1}{\partial z}\,\bar{i}_z$$

$$\Phi_1=\sum_n\int_{-\infty}^{\infty}d\omega\,\Phi_{\omega n}\,e^{j(\omega t-\beta_n(\omega)z)} \tag{16}$$

$$f_1=-\frac{e}{m}\frac{\partial f_o}{\partial v}\sum_n\int_{-\infty}^{\infty}d\omega\,\Phi_{\omega n}\frac{\beta_n(\omega)}{\omega-\beta_n(\omega)v}\,e^{j(\omega t-\beta_n(\omega)z)}. \tag{17}$$

In Eqs. 16 and 17 we have written the linearized solutions (E_1, f_1) as a sum over elementary traveling waves. The sum over n is taken over the different branches of the dispersion function $\beta_n(\omega)$. Only one of these branches is taken to be convectively unstable. The quantity $\Phi_{\omega n}$ is the "Fourier coefficient" of the linearized solution at the real frequency ω. This coefficient describes the initial excitation of Φ_1 at $z = 0$, when the beam first enters the interaction region. Note that since Φ_1 must be a real function,

$$\Phi^*_{\omega n} = \Phi_{-\omega n}.$$

The diffusion coefficient D will now be evaluated. From (14a),

$$D = +\frac{e}{m}\langle E_1 f_1\rangle \left(\frac{\partial f_o}{\partial v}\right)^{-1}. \tag{18}$$

Using (16) and (17), and doing the time average, we have

$$D = +\frac{e^2}{m^2} \sum_n \sum_{n'} \int d\omega \int d\omega' \, E_{n\omega} E_{n'\omega'} \frac{j}{\omega' - \beta_{n'}(\omega')v} e^{-j(\beta_n(\omega)+\beta_{n'}(\omega'))z} \frac{1}{j(\omega+\omega')T_o} \left(e^{j(\omega+\omega')T_o} - 1\right) \tag{19}$$

or

$$D = \sum_{n,n'} D_{nn'}. \tag{20}$$

Here we have written

$$E_{n\omega} \equiv j\beta_n(\omega)\,\Phi_{\omega n}. \tag{21}$$

Physically, the double sum over n and n' represents a summation over all the waves present in the one-dimensional system. Only one of these waves, say $n = 1$, is assumed to be convectively unstable. Let the maximum gain $\left|\text{Im } \beta_1(\omega)\right|_{max}$ of this unstable wave be γ. For $\gamma z \lesssim 1$, the unstable wave has not greatly increased in amplitude over its initial value at $z = 0$. Therefore, physically, we expect each term in the sum (20) to be equally important; the contributions of the purely propagating or evanescent waves to D for $\gamma z \lesssim 1$ cannot be neglected. On the other hand, for $\gamma z \ll 1$, the amplitude of the unstable wave has increased greatly over its initial value at $z = 0$. This should manifest itself by an increase in the diffusion term D_{11}. For γz sufficiently large, we expect the term D_{11} to be much larger than any of the other terms $D_{nn'}$ in the sum (20).

Note that there is an upper limit L on the size of γz. If $\gamma z \gtrsim L$, then f_1 becomes comparable in magnitude to f_o, and the whole procedure of quasi-linear theory, in which the right-hand sides of (12) and (13) are assumed small, is invalid. The upper limit L is set by the magnitude of the initial excitation $\Phi_{\omega n}$. If $\Phi_{\omega n}$ is "small enough," then $L \gg 1$. We then assert that

$$D(z, v) \approx D_{11} \tag{22a}$$

within the range

$$1 \lesssim \gamma z \lesssim L. \tag{22b}$$

The diffusion term D_{11} is given by

$$D_{11} = \frac{e^2}{m^2} \int d\omega \int d\omega' \, E_\omega E_{\omega'} \, j \frac{1}{\omega' - \beta(\omega')v} \, e^{-j(\beta(\omega)+\beta(\omega'))z} \, \frac{1}{j(\omega+\omega')T_o} \left(e^{j(\omega+\omega')T_o} - 1 \right). \tag{23}$$

The gain Im $\beta(\omega)$ of the unstable wave has a positive peak γ at $\omega = \omega_o$ and $\omega = -\omega_o$, as shown in Fig. X-19. Let us expand the dispersion function $\beta(\omega)$ in a Taylor series around ω_o and $-\omega_o$:

$$\begin{aligned} \beta(\omega_o+s) &= q + \frac{1}{v_g} s + \dots + j\left(\gamma - \frac{1}{2} c_o s^2 + \dots\right) \\ \beta(-\omega_o-s) &= -q - \frac{1}{v_g} s - \dots + j\left(\gamma - \frac{1}{2} c_o s^2 + \dots\right) \end{aligned} \tag{24}$$

in which by definition,

$$\frac{1}{v_g} \equiv \left. \frac{\partial(\mathrm{Re}\,\beta)}{\partial\omega} \right|_{\omega_o} \tag{25}$$

$$c_o \equiv - \left. \frac{\partial^2(\mathrm{Im}\,\beta)}{\partial\omega^2} \right|_{\omega_o} . \tag{26}$$

The bandwidth $\Delta\omega$ thus appears in a natural manner from these expansions:

$$\Delta\omega \equiv \sqrt{\frac{2\gamma}{c_o}} . \tag{27}$$

For $\gamma z \gg 1$, the exponential space factor of the integrand in (23) is peaked near $\omega = \pm\omega_o$ and $\omega' = \pm\omega_o$. From the inequalities (5), one can thus write (23) in the form

$$D_{11} = \frac{e^2}{m^2} (I_1 + I_2), \tag{28}$$

where

$$I_1 = \int_{(\omega_o)} d\omega' \int_{(-\omega_o)} d\omega \, jE_\omega E_{\omega'} \frac{1}{\omega' - \beta(\omega')v} \, e^{-j(\beta(\omega)+\beta(\omega'))z} \tag{29}$$

and

$$I_2 = \int_{(-\omega_o)} d\omega' \int_{(\omega_o)} d\omega\, jE_\omega E_{\omega'} \frac{1}{\omega' - \beta(\omega')v} e^{-j(\beta(\omega)+\beta(\omega'))z}. \tag{30}$$

In (29) we let $\omega' = \omega_o + s$ and $\omega = -\omega_o - t$, use the expansions (24), and do the s and t integrations to obtain

$$I_1 = j\pi \left|E_{\omega_o}\right|^2 \sqrt{\frac{2}{c_o z}}\, e^{\left(2\gamma - \frac{1}{c_o v_g^2}\right)z} Z\left(\sqrt{\frac{c_o z}{2}}\left(qv - \omega_o + j\gamma v + j\frac{1}{c_o v_g}\right)\right), \tag{31}$$

where $Z(y_o)$ is the plasma dispersion function, tabulated by Fried and Conte.[4]

Let us return to (30), the other half of D_{11}. Setting $\omega' = -\omega_o - s$ and $\omega = \omega_o + t$ in this integral and using the expansions (24), we obtain

$$I_2 = I_1^*. \tag{32}$$

Thus

$$D_{11}(\gamma z \gg 1) = -\frac{2\pi e^2}{m^2} \frac{\Delta\omega}{\sqrt{\gamma z}} \left|E_{\omega_o}\right|^2 e^{\left(2\gamma - \frac{(\Delta\omega)^2}{2\gamma v_g^2}\right)z} \operatorname{Im} Z\left(\frac{\sqrt{\gamma z}}{\Delta\omega}\left(qv - \omega_o + j\gamma v + j\frac{(\Delta\omega)^2}{2\gamma v_g}\right)\right). \tag{33}$$

The terms in $(\Delta\omega)^2$ can usually be neglected, since $\Delta\omega$ is assumed small. Furthermore, for most systems, the argument of the Z function is much larger than unity, even at resonance $v = \omega_o/q$, unless the gain γ is very small. Expanding the Z function in an asymptotic series, one obtains a simplified form for the diffusion coefficient D:

$$D_{11}(\gamma z \gg 1) = -\frac{2\pi e^2}{m^2} \left|E_{\omega_o}\right|^2 (\Delta\omega)^2 \frac{e^{2\gamma z}}{\gamma z} \frac{\gamma v}{(\omega_o - qv)^2 + \gamma^2 v^2}. \tag{34}$$

Note that (34) has a singularity in the limit as $\gamma z \to 0$; however, D_{11} is not correctly given by (34) in this limit. In fact, we shall neglect the diffusion of the beam in the region $\gamma z \lesssim 1$.

c. Beam Diffusion in the Steady State

Assume that at $t = 0$, an electron beam is injected into a semi-infinite interaction region. After the initial transients have died out, the beam will reach a steady state, in which the velocity diffusion of the beam will be a function of the distance z from the beam entrance plane $z = 0$. Accordingly, we set $\frac{\partial}{\partial t} \equiv 0$ in the diffusion equation to obtain

$$v\frac{\partial f_o}{\partial z} + \frac{\partial}{\partial v}\left(D(z,v)\frac{\partial f_o}{\partial v}\right) = 0, \tag{35}$$

where D(z, v) is given by (33) or (34). One can demonstrate the following properties concerning all distribution functions f_o that satisfy (35):

1. The number of beam electrons is conserved. Proof: Integrate (35) over all velocity space.

2. The distribution function has a velocity derivative $(\partial f_o/\partial v)_{v=0}$ which is zero for any z. Proof: Expand (35) and take the limit $v \to 0$, using (34) to evaluate the limiting form of the diffusion coefficient D.

3. Beam electrons are never reflected or "turned around" in velocity space. Proof: Integrate (35) over negative velocities and use 2.

4. Assume that the entering beam is monoenergetic at $\gamma z \lesssim 1$. Then initially, the beam loses power provided $v_o > \omega/q$. Proof: The power flow p(z) is given by

$$p(z) = \int_0^\infty dv\, v^3 f_o(v, z).$$

Multiply (35) by v^2 and integrate over positive velocities. The second term can be integrated by parts twice to yield

$$\left(\frac{\partial p}{\partial z}\right)_{\gamma z \lesssim 1} = -\frac{\partial}{\partial v}(vD(z, v))_{v=v_o}$$

From (34), it then follows that

$$\left(\frac{\partial p}{\partial z}\right)_{\gamma z \lesssim 1} < 0,$$ provided $v_o > (\omega_o/q)$ which is the condition for the existence of a convective instability. Q. E. D.

Computations on the diffusion of f_o for a particular example are at present in progress.

M. A. Lieberman, A. Bers

References

1. R. J. Briggs, Electron-Stream Interaction with Plasmas (The M.I.T. Press, Cambridge, Mass., 1964). The interaction of a filamentary electron beam with a cold-plasma waveguide gives rise to a narrow-bandwidth convective instability for frequencies slightly below the upper hybrid. As another example, the interaction of an electron beam with a slow-wave structure, as in a traveling-wave tube, can give rise to a narrow-bandwidth, convective instability.

2. Quarterly Progress Report No. 79, Research Laboratory of Electronics, M.I.T., October 15, 1965, pp. 118-126.

3. W. E. Drummond and D. Pines, "Non-linear Stability of Plasma Oscillations," Nuc. Fusion 1962, Suppl. Part 3, pp. 1049-1057. In the usual technique of quasi-linear theory, $\overline{\beta}$ is considered to be purely real, and ω is complex. This technique is not suitable for the study of convective instability.

4. B. Fried and S. Conte, The Plasma Dispersion Function (Academic Press, New York, 1961).

7. WAVE-MIRROR HEATING

In our last report,[1] we looked at the heating of electrons reflecting off hard walls (idealized magnetic mirrors) in the presence of a longitudinal traveling wave. We found that this heating could be considerable, if the walls were perfectly reflecting or if the electrons bounced back from the walls with a phase random to the entering phase.

Computer experiments were run to check the theory, since a number of approximations had been made. The heating arising from the hard walls and the random phase of the re-entry model was even greater than expected (Fig. X-20).

Computer experiments were also run with a more realistic model of the mirrors. For a wave varying as $\cos(\omega t - kz)$, distances were normalized to k^{-1}, times to ω^{-1}.

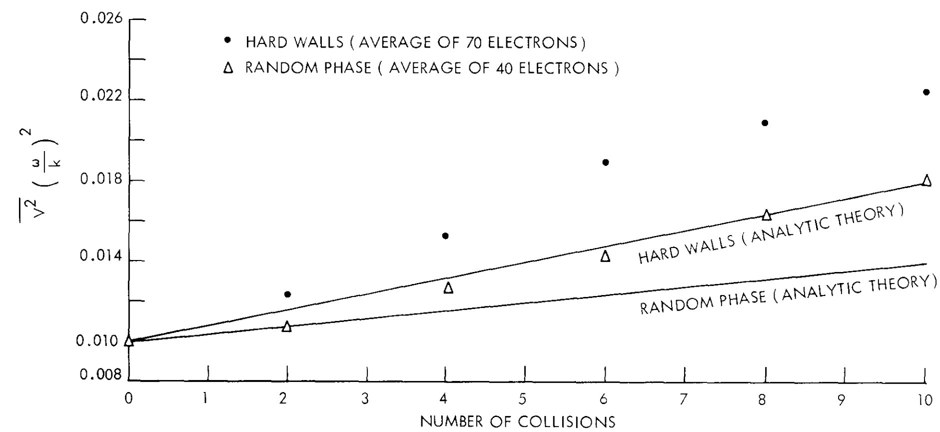

Fig. X-20. Average energy gain vs number of wall collisions. (Hard walls and random phase of re-entry.)

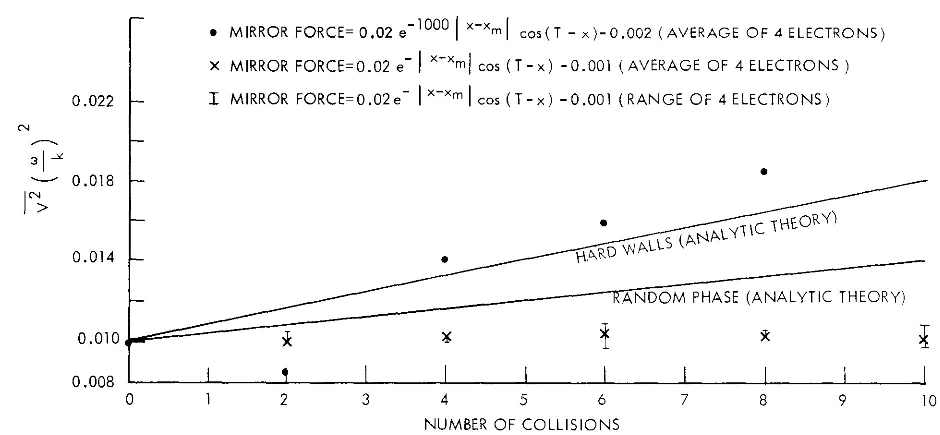

Fig. X-21. Average energy gain vs number of mirror collisions. (Constant decelerating force in mirrors, with exponentially decaying waves.)

The wave (normalized), varied as 0.02 cos (t-x) between the mirrors, and as $0.02\, e^{-a|x-x|_m} \cos(t-x) \pm .001$ in the mirrors. The initial velocity in all cases was $0.1\ \omega/k$. The results for a = 1000 and a = 1 are shown in Fig. X-21. For a = 1000, the results are about the same as for the random phase theory. For a = 1, however, the heating is practically nonexistent. Similar results occur for a = 0.1 and a = 0. For the a = 1 case, the maximum point of penetration into the mirrors is $5k^{-1}$, less than a wavelength. The time involved in reflection was ≈ 30 oscillation periods.

The results are physically plausible. For hard walls or a random-phase model, an electron can be accelerated for a half-period, reflected, and accelerated for another half-period, since both the velocity and field have changed sign. For more realistic mirrors, the electron spends several periods in being reflected. Each half-period is then almost exactly cancelled by the next half-period.

Since the wavelength in a beam-plasma system is normally small compared with the mirror dimensions, it seems unlikely that this kind of heating is important.

J. A. Davis

References

1. J. A. Davis, Quarterly Progress Report No. 80, Research Laboratory of Electronics, M.I.T., January 15, 1966, pp. 120-124.

8. THEORY OF PLASMA EXCITATION BY A LINE-CHARGE SOURCE

As a first step in understanding the excitation of the beam-plasma discharge (BPD) by a modulated beam[1,2] we consider the following theoretical model: Assume a linearized hydrodynamic representation of the fully ionized macroscopically neutral two-component plasma, with a longitudinal DC magnetic field, $B_o\bar{i}_z$. The unbounded plasma is excited by a sinusoidally varying line charge oriented parallel to the DC magnetic field, $\rho = \rho_o\delta(x)\delta(y)$, for exp(jωt) sinusoidal steady-state time dependence. The constant ρ_o has units of coulombs per meter. We are interested in quasi-static solutions that have azimuthal symmetry and no longitudinal variation.

The linearized transport equations are

$$j\omega m_e N_o \bar{v}_e = -N_o e(\bar{E}+\bar{v}_e \times B_o \bar{i}_z) - m_e u_e^2 \nabla n_e \tag{1}$$

$$j\omega m_i N_o \bar{v}_i = N_o e(\bar{E}+\bar{v}_i \times B_o \bar{i}_z) - m_i u_i^2 \nabla n_i, \tag{2}$$

with the linearized equations of continuity

$$N_o \nabla \cdot \overline{v}_e = -j\omega n_e \tag{3}$$

$$N_o \nabla \cdot \overline{v}_i = -j\omega n_i \tag{4}$$

$$\nabla \cdot \overline{E} = \frac{\rho_o}{\epsilon_o} \delta(x)\delta(y) + \frac{e}{\epsilon_o}(n_i - n_e). \tag{5}$$

Introduce a scalar potential Φ, where

$$\overline{E} = -\nabla\Phi. \tag{6}$$

We are interested in solutions for which $E_z = 0$, and $v_{ez} = v_{iz} = 0$, leaving seven unknowns Φ, n_e, n_i, v_{ex}, v_{ey}, v_{ix}, and v_{iy}.

The set of seven equations is solved by using Fourier transform theory, and the following transform pair:

$$\begin{aligned} f(x,y) &= \frac{1}{(2\pi)^2} \int_{-\infty}^{\infty} \int_{-\infty}^{\infty} f(k_x, k_y)\, e^{-jk_x x - jk_y y}\, dk_x\, dk_y \\ f(k_x, k_y) &= \int_{-\infty}^{\infty} \int_{-\infty}^{\infty} f(x,y)\, e^{jk_x x + jk_y y}\, dx\, dy. \end{aligned} \tag{7}$$

The solutions for the transformed equations are

$$n_e = \frac{\rho_o}{e} \omega_{pe}^2 \left[\frac{\left(k_T^2 u_i^2 - \omega^2 + \omega_{ci}^2\right)}{D(k_x, k_y)} \right] \tag{8}$$

$$n_i = \frac{-\rho_o}{e} \omega_{pi}^2 \left[\frac{\left(k_T^2 u_e^2 - \omega^2 + \omega_{ce}^2\right)}{D(k_x, k_y)} \right] \tag{9}$$

$$\Phi = \frac{\rho_o}{\epsilon_o} \left[\frac{\left(k_T^2 u_i^2 - \omega^2 + \omega_{ci}^2\right)\left(k_T^2 u_e^2 - \omega^2 + \omega_{ce}^2\right)}{k_T^2 D(k_x, k_y)} \right] \tag{10}$$

$$v_{ex} = -\frac{\rho_o e}{m_e \epsilon_o} \left[\frac{\left(\omega k_x + j\omega_{ce} k_y\right)\left(k_T^2 u_i^2 - \omega^2 + \omega_{ci}^2\right)}{k_T^2 D(k_x, k_y)} \right] \tag{11}$$

$$v_{ey} = -\frac{\rho_o e}{m_e \epsilon_o} \left[\frac{\left(\omega k_y - j\omega_{ce} k_x\right)\left(k_T^2 u_i^2 - \omega^2 + \omega_{ci}^2\right)}{k_T^2 D(k_x, k_y)} \right] \tag{12}$$

$$v_{ix} = \frac{\rho_o e}{m_i \epsilon_o} \left[\frac{\left(\omega k_x - j\omega_{ci} k_y\right)\left(k_T^2 u_e^2 - \omega^2 + \omega_{ce}^2\right)}{k_T^2 D(k_x, k_y)} \right] \tag{13}$$

$$v_{iy} = \frac{\rho_o e}{m_i \epsilon_o} \left[\frac{\left(\omega k_y + j\omega_{ci} k_x\right)\left(k_T^2 u_e^2 - \omega^2 + \omega_{ce}^2\right)}{k_T^2 D(k_x, k_y)} \right]. \tag{14}$$

Here, $D(k_x, k_y)$ is the dispersion relation[3] given by

$$D(k_x, k_y) = \left(k_T^2 u_i^2 - \omega^2 + \omega_{ci}^2 + \omega_{pi}^2\right)\left(k_T^2 u_e^2 - \omega^2 + \omega_{ce}^2 + \omega_{pe}^2\right) - \omega_{pe}^2 \omega_{pi}^2 , \tag{15}$$

where

$$k_T^2 = k_x^2 + k_y^2. \tag{16}$$

The quantities of Eqs. 8-14 are the spatial Fourier transforms of the first-order densities, potential, and velocities caused by the sinusoidally varying line charge. The responses as a function of x and y are obtained by taking the inverse Fourier transforms as given in Eq. 7. This work is at present in progress.

G. D. Bernard, A. Bers

References

1. L. D. Smullin, "Beam-Plasma Discharge: Excitation of Ions at the Ion Cyclotron Frequency (Theory)," Quarterly Progress Report No. 80, Research Laboratory of Electronics, M.I.T., January 15, 1966, pp. 111-113.
2. W. D. Getty and G. D. Bernard, "Beam-Plasma Discharge: Excitation of Ions at the Ion Cyclotron Frequency (Experiment)," Quarterly Progress Report No. 80, Research Laboratory of Electronics, M.I.T., January 15, 1966, pp. 113-115.
3. W. P. Allis, S. J. Buchsbaum, and A. Bers, Waves in Anisotropic Plasmas (The M.I.T. Press, Cambridge, Mass., 1963), p. 76, Eq. (5.44).

9. EXPERIMENTAL INVESTIGATION OF INSTABILITIES IN AN ELECTRON BEAM WITH TRANSVERSE ENERGY

Calculations of Bers and Gruber have predicted instabilities in an electron beam confined by a magnetic field if the electrons have enough transverse energy.[1] To find the optimum conditions for the instabilities, it was necessary to plot the dispersion relation for different values of the plasma frequency ω_p and of the parameter $k_\perp v_{0\perp}/\omega_c$ ($k_\perp$ = propagation constant perpendicular to the magnetic field, $v_{0\perp}$ = transverse velocity of the electrons, ω_c = cyclotron frequency).[2] These resulting figures show that an instability can be expected in a plasma at $\omega = 0.6\ \omega_c$ or in a beam at $\omega = 0.6\ \omega_c + k_{\parallel} v_{0\parallel}$ ($k_{\parallel}$ and $v_{0\parallel}$ are the propagation constant and electron velocity parallel to the magnetic field). The necessary condition for the plasma frequency is $\omega_p > 0.6\ \omega_c$. If $\omega_p = 0.7\ \omega_c$, the ratio of the propagation constants parallel and perpendicular to the beam will be $k_{||}/k_{\perp} \geq 2$. In a cylindrical beam surrounded by a metal cylinder the electric field of the wave should have a transverse dependence proportional to the Bessel function $J_0(k_{\perp}r)$. For a metal cylinder of radius 1.2 cm, it follows that $k_{\perp} = 2/\text{cm}$ and $k_{||} \geq 4/\text{cm}$. With a magnetic field of 70 gauss ($f_c = 200$ Mc/sec) and a velocity of the electrons corresponding to 100 V, the instability should occur at a frequency of 600 Mc/sec or higher. This value is only an estimation because the theory assumes infinite transverse dimensions of the beam.

For the experiment two tubes were built (Fig. X-22). They are mounted inside a solenoid producing a constant magnetic field. A gap of 1 cm in the solenoid is located immediately before the phosphor-coated collector to allow the observation of the beam striking the collector and the detection of any RF signal. Two grids are mounted in front of the cathode so that the beam voltage and the beam current can be varied independently.

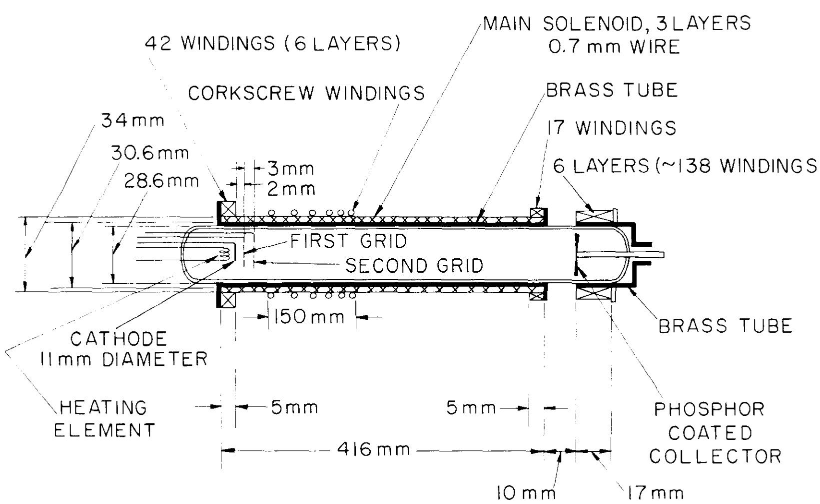

Fig. X-22. Schematic diagram of the experimental tube.

A fraction of the total kinetic energy of the electrons is converted into transverse energy by a corkscrew device.[3] Two corkscrews were designed and built for a magnetic field of 70 gauss and 100 gauss. The corkscrews decelerate electrons starting at a beam voltage of 150 V, converting one-third of the electron energy into transverse energy. The electrons leaving the corkscrew spiral around in orbits of 7-mm diameter at 70 gauss and 5-mm diameter at 100 gauss.

The first tube was built to check the corkscrew device. In this tube the second grid is replaced by a plate with three small holes at different radial distances from the axis of symmetry. The three holes produce three thin beams and three points on the collector. The corkscrew transforms the three points into three circles with a diameter of 7 mm or 5 mm. The corkscrew device worked very well. Small deviations from the correct values of the magnetic field, beam voltage, and corkscrew current were admissible.

Under the assumption of a beam cross section equal to that of the cathode (1 cm^2), the necessary current at 70 gauss, 100 V, and $\omega_p = 0.7\ \omega_c$ is 23 mA. Thus the perveance of the beam is $23 \cdot 10^{-6}\ I/V^{3/2}$, which is close to the highest possible perveance. This value could not be reached with the tube, however, since the beam becomes unstable at 15 mA and spreads out. Operating at lower magnetic field should permit lower current density, but unfortunately the magnetic field is then too small for sufficient confinement of the beam.

No oscillation was found at the expected frequencies, but the tube showed strong oscillations at 250 Mc/sec when working without the corkscrew. In this case the tube acts as a double-stream amplifier. The rate of back-scattered electrons from the collector[4] with sufficient energy is high enough to form a second beam confined by the magnetic field. This beam flows toward the cathode and is reflected again by the cathode (or grid) potential.

To find the predicted instabilities, it appears that higher beam densities are necessary. One possible way of achieving this is to use a neutralized beam. This work will continue either at M.I.T. or at the Technical University of Berlin.

G. Bolz

References

1. A. Bers and S. Gruber, Appl. Phys. Lett. 6, 27 (1965).
2. G. Bolz, Quarterly Progress Report No. 80, Research Laboratory of Electronics, M.I.T., January 15, 1966, pp. 135-136.
3. R. C. Wingerson, T. H. Dupree, and D. Rose, Phys. Fluids 7, 1475 (1964).
4. E. J. Sternglass, Phys. Rev. 95, 345 (1954).

10. HIGH-FREQUENCY ELECTRON-PHONON INTERACTIONS IN A MAGNETIC FIELD

Bers and Musha have previously reported[1] the classical dispersion relation for electrons interacting with acoustic waves in a solid. They considered parallel electric and magnetic fields in the quasi-static approximation. Taking the deformation potential as the coupling between the electron and phonon systems, they found the dispersion relation

$$K_p + K_e - 1 = 0, \tag{1}$$

where

$$K_p = \frac{\omega^2 - q^2 s^2}{\omega^2 - q^2 s^2 + \frac{c^2 \epsilon_L}{\rho e^2} q^4} \tag{2}$$

$$K_e = 1 - \frac{\omega_p^2}{q^2} \frac{\int_{-\infty}^{\infty} dw_{\parallel} \int_0^{\infty} dw_{\perp} w_{\perp} 2\pi \sum_n \frac{J_n^2(p)\left(\frac{n\omega_c}{w_{\perp}} \frac{\partial f_{01}}{\partial w_{\perp}} - q_{\parallel} \frac{\partial f_{01}}{\partial w_{\parallel}}\right)}{(\omega+i\nu-q_{\parallel}w_{\parallel}-n\omega_c)}}{1 + i\nu \int_{-\infty}^{\infty} dw_{\parallel} \int_0^{\infty} dw_{\perp} w_{\perp} 2\pi f_0 \sum_n \frac{J_n^2(p)}{(\omega+i\nu-q_{\parallel}w_{\parallel}-n\omega_c)}}. \tag{3}$$

Here, s is the sound velocity, ω_p is the electron plasma frequency, ω_c is the electron cyclotron frequency, $q_{\parallel}$ is the wave-number component along B_0, $q_{\perp}$ is the wave-number component across B_0, and $p = q_{\perp}w_{\perp}/\omega_c$; ν is the electron-lattice collision frequency, and phonon decay is ignored in Eq. 2.

We have been analyzing the instabilities predicted by these equations for parameters typical of InSb at 77°K with an effective deformation potential coupling constant taken to be 30 ev.[2] For these parameters Maxwell-Boltzmann statistics are appropriate and we assume:

$$f_0 = \frac{1}{(2\pi)^{3/2} v_T^3} \exp -\left(w_{\perp}^2+w_{\parallel}^2\right) \Big/ 2v_T^2 \tag{4}$$

$$f_{01} = \frac{1}{(2\pi)^{3/2} v_T^3} \exp -\left(w_{\perp}^2+(w_{\parallel}-v_D)^2\right) \Big/ 2v_T^2, \tag{5}$$

where v_T is the thermal velocity, and v_D is the drift velocity.

The imaginary part of the frequency, ω, for real wave vector, $\bar{q}$, has been computed as a function of the angle of propagation for various values of electric and magnetic fields with the aid of Project MAC CTSS. The results are shown in Fig. X-23.

Taking the appropriate values of the parameters, we find that ω may be considered to be purely real in Eq. 3, as $\omega_i \gg \nu$. The computations were carried out with this approximation.

Since the electron-phonon interaction has a relatively small effect on the unperturbed electron and phonon systems, $\omega_i \ll \omega_r \approx q_r s$ and Re $K_e \gg 1$. In this approximation the dispersion relation may be solved explicitly for the growth rate of phonons:

$$\omega_i \approx \frac{C^2\epsilon_L}{\rho e^2}\frac{q^3}{s}\,\mathrm{Im}\,(K_e). \tag{6}$$

The physics of the interaction and the results of our more exact computations may be readily interpreted from this approximate description. For the high frequencies that

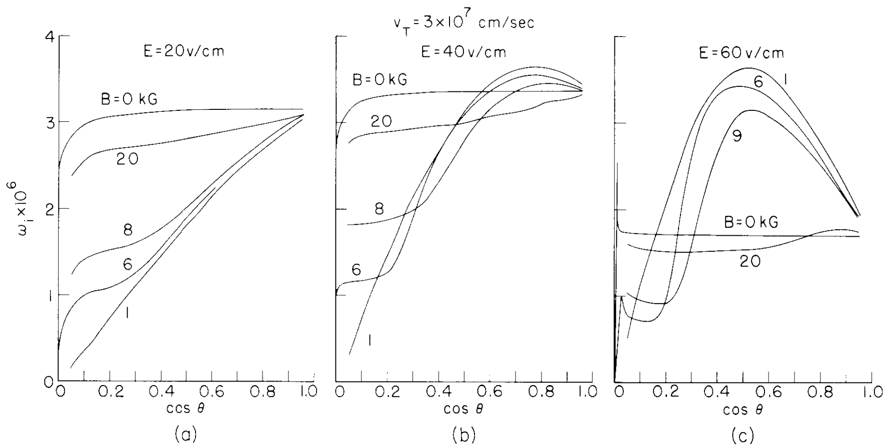

Fig. X-23. Variation of amplification with direction of propagation. The variation for very small cos θ has been included only for B = 0 kg and B = 6 kg. (a) v_D much less than v_T. (b) v_D slightly greater than v_T. (c) v_D much greater than v_T.

we are considering, the mean-free path of the electrons is large compared with a phonon wavelength ($qv_T/\nu \gg 1$). Thus the major contribution to Im (K_e) that gives rise to growth comes from anti-Landau damping, and the effect of collisions is usually small.

a. Zero Magnetic Field

In the limit of zero magnetic field, the expression for K_e reduces to

$$K_e = 1 + \frac{\dfrac{\omega_p^2}{q^2}\displaystyle\int_{-\infty}^{\infty} dw_{\|}\int_0^{\infty} dw_{\perp}\,\frac{w_{\perp}2\pi q_{\|}\dfrac{\partial f_{01}}{\partial w_{\|}}}{(\omega+i\nu-q_{\|}w_{\|})}}{1+i\nu\displaystyle\int_{-\infty}^{\infty} dw_{\|}\int_0^{\infty} dw_{\perp}\,\frac{w_{\perp}2\pi f_o}{(\omega+i\nu-q_{\|}w_{\|})}} \tag{7}$$

and the general behavior of ω_i versus angle can be explained on the basis of anti-Landau damping. The most interesting feature of these curves is the sharp peak in the amplification that occurs for propagation almost across the field when $v_D > v_T$. This peak occurs at just that angle where one would expect the largest Landau damping effect, namely $\cos\theta = \frac{\omega}{qv_T}$, as can be seen from Fig. X-24.

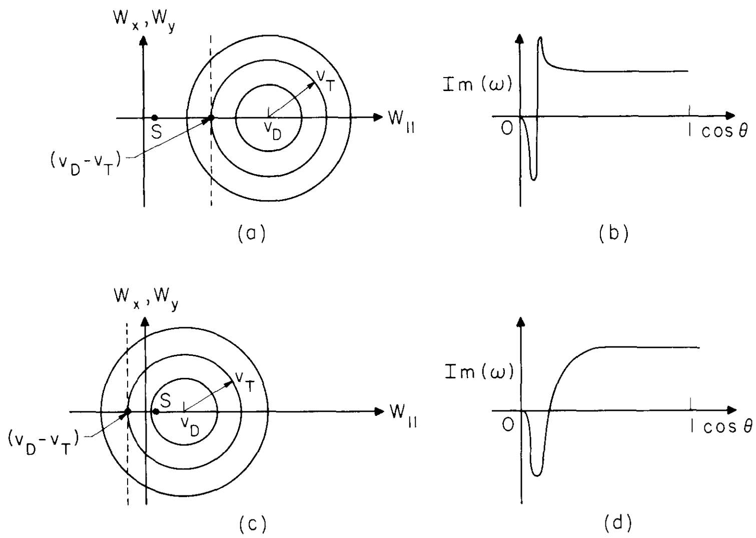

Fig. X-24. (a) Distribution function, f_{01}, for $v_D > (v_T+s)$. Circles represent loci of constant f_{01}. $\frac{\partial f_{01}}{\partial w_{\parallel}}$ is maximum along the dotted line ($w_{\parallel} = v_D - v_T$). (b) Expected variation of the amplification with angle of propagation for the case represented in (a). (c) Same as (a) except that $v_D < v_T$. (d) Expected variation in the amplification for the case represented in (c). Note that there is no peak in the amplification for propagation almost transverse to the field as was the case in (b).

The maximum Landau damping effect is expected when the electrons along the line ($v_D - v_T$) (maximum slope of the distribution function) are moving in the direction of wave propagation with a velocity equal to the phase velocity of the wave. Also, damping is expected whenever there are more electrons moving infinitesimally slower that the wave than are moving infinitesimally faster than the wave; this condition is satisfied for $\cos\theta \leq \frac{\omega}{qv_D}$. Mathematically this is contained in the dispersion relation, in that $\frac{\partial f_{01}}{\partial w_{\parallel}}$ must be evaluated at the pole of the denominator, i.e., $\cos\theta = \frac{\omega}{qw_{\parallel}}$, neglecting collisions. Thus as $\cos\theta$ varies from 0 to 1, $w_{\parallel}$ varies from ∞ to s and the general form of the growth as a function of $\cos\theta$ is shown in Fig. X-24.

b. Finite Magnetic Field

When a magnetic field is applied the situation becomes more complicated. One physical process that can be identified in these curves (Figs. X-23b and c) is that of Doppler-shifted cyclotron resonance. This comes in through the resonant denominator in the integrals of Eq. 3. According to Eq. 6, the amplification will be maximum when the angle of propagation is such that

$$\sum_n J_n^2(p)\left(\frac{n\omega_c}{w_\perp}\frac{\partial f_{01}}{\partial w_\perp} - q_{||}\frac{\partial f_{01}}{\partial w_{||}}\right)$$

is maximum at the pole of the denominator. For low magnetic fields (≈ 1 kgauss) none of the terms of this expression dominate and hence a large number of terms in the series must be taken into account and the position of the peak cannot be given by any simple formula. For moderate magnetic fields (≈ 6 kgauss), the parameters are such that the Bessel functions decrease rapidly with increasing order and hence the major effect is given by the first term. Also, $\frac{\omega_c}{w_\perp}\frac{\partial f_{01}}{\partial w_{||}}$ is much larger than $q_{||}\frac{\partial f_{01}}{\partial w_{||}}$. Hence the maximum is given by $w_{||} = v_D$ or $\cos\theta = \frac{\omega+\omega_c}{qv_D}$, with collisions neglected.

For $v_T > v_D$, the amplification does not rise over the zero magnetic field value for any magnetic field (Figs. X-23, X-25 and X-26). For high magnetic fields this can be explained by noting that the condition given above for Doppler-shifted cyclotron resonance cannot be met for $0 \leqslant \cos \leqslant 1$. We do not yet fully understand the situation for lower

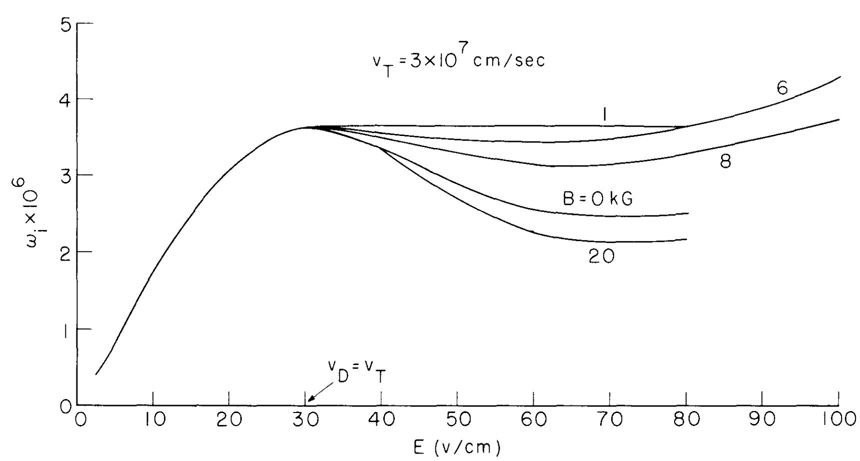

Fig. X-25. Maximum (with respect to angle) amplification vs electric field, with the magnetic field as a parameter.

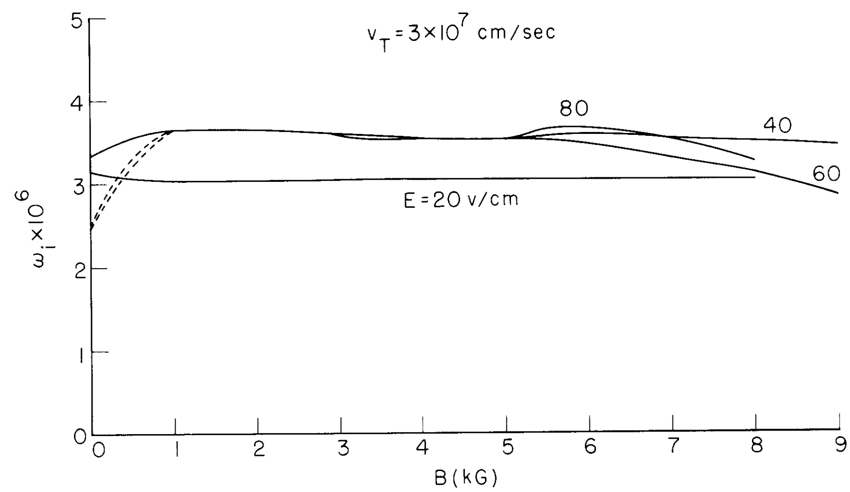

Fig. X-26. Maximum (with respect to angle) amplification vs magnetic field, with the electric field as a parameter.

magnetic fields. Note that $v_T > v_D$ is the usual situation in a solid; when the electric field is increased in order to increase v_D, v_T also increases because of the high collision rate. As can be seen from Fig. X-25, for $v_D < v_T$ the growth rate is independent of the applied magnetic field.

Work is now under way to determine the nature of these instabilities — whether they are absolute or convective. Also, the quantum-mechanical formulation of the dispersion relation, given by Bers and Musha,[1] is being examined to determine the specifically quantum-mechanical aspects of the interaction and when they may be important.

A. Bers, S. R. J. Brueck

References

1. A. Bers and T. Musha, Quarterly Progress Report No. 79, Research Laboratory of Electronics, M.I.T., October 15, 1965, p. 104.
2. Recent measurements at Lincoln Laboratory, M.I.T., indicate that the dominant electron-phonon coupling mechanism in InSb at 9 kMc is piezoelectric rather than deformation potential (Kenneth Hill, private communication).

X. PLASMAS AND CONTROLLED NUCLEAR FUSION*

B. Applied Plasma Physics Related to Controlled Nuclear Fusion

Research Staff

Prof. D. J. Rose
Prof. T. H. Dupree
Prof. L. M. Lidsky
Prof. E. P. Gyftopoulos
L. M. Lontai

Graduate Students

R. W. Flynn
R. A. Hill
C. S. Ribbeck
C. E. Wagner
D. R. Wilkins
J. C. Woo
N. D. Woodson

1. THERMONUCLEAR REACTOR: INTRODUCTORY SYSTEM ANALYSIS

Considerable work has been done on investigating various controlled thermonuclear power devices. Plasma physics problems are still to be solved before fusion power will be available, but it is evident already that the engineering aspects of the problem will be very challenging. The results of an engineering analysis may alter the direction and intensity of the controlled thermonuclear power program.

The present study concentrates first on general comparisons of steady-state and pulsed devices. Following this, specific introductory engineering analyses involving the magnitude of the leakage of the magnetic field into the coolant of a pulsed device, the temperature distribution in the vacuum wall of a pulsed device of small radius, and power-generating cost estimates are presented.

The study of the magnetic leakage was an extension of the work performed by Ribe and co-workers.[1] Ribe's device has a 10-cm vacuum wall radius and a maximum B field of 200 kgauss. Ribe presents data for a given magnetic pulse, $B_{max} = 200$ kgauss, showing the diffusion of the magnetic field into a conductor as a function of time. With these data, an approximate value of the average magnetic field within the conductor as a function of time may be found. Thus, if the conductor is a liquid-metal coolant, we shall have the value of the magnetic field through which the coolant will be pumped. The results show that for a 50-cm coolant thickness, the average field is approximately 20% of the maximum field (200 kgauss) initially, and drops to approximately 10% of the maximum after a typical heat time (500 msec) has elapsed. The power required to pump the liquid-metal coolant through this field will be enormous. Thus, a fused salt still appears to be the best coolant available.

Our small-radius vacuum-wall study continues Dean's work,[2] to reach new conclusions. Dean proposed to examine the Bremsstrahlung radiation absorption with a model

*This work was supported principally by the National Science Foundation (Grant GK-614).

that approximates the actual attenuation of the radiation. This model assumes that the Bremsstrahlung is not a surface heat flux, but is instead absorbed within a small volume just inside the wall.

By using this model and equations derived by Carslaw and Jaeger,[3] temperature distributions can be obtained as functions of space and time. For a Copper inner wall of 1-cm thickness and 10-cm radius, we found that the temperature rise attributable to the Bremsstrahlung from a single 0.04-sec pulse is approximately 105°C. Similarly, the temperature rise caused by neutron heating is approximately 200°C at the inner face of the wall. Next, the energy dissipation during the dead time is examined. By calculating the temperature drop after the initial peak, we found that approximately 70% of the initial energy input remains in the wall at the end of the dead time. Thus the following pulses tend to build up on one another and approach a quasi-steady state. It is estimated that for the wall under consideration, this average steady state at the inner face will be approximately 1000°C above the initial level of 600°C, which melts Copper and seriously damages any other material considered. The temperature distribution for a single pulse will be superimposed over this average, as shown in Fig. X-28.

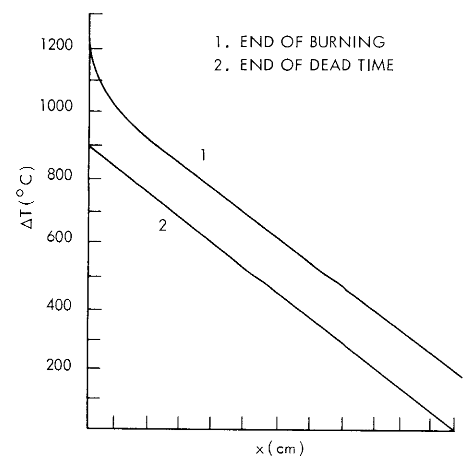

Fig. X-28. Vacuum-wall temperature distribution.

Returning to large-vacuum walls, of approximately 1-meter radius, the economic considerations of thermonuclear devices are developed. The costs presented represent the power plant up to the heat exchanger, but not beyond. Under the assumption that Tritium has no value and, therefore, no costs of separation accrue, injection is performed by 5-amp ion guns valued at $40,000 per gun, burn-up in a steady-state device is 0.5, (while in a pulsed device burn-up is 0.1), the final cost will be approximately 0.5 M/kWhe for either system. Steady-state device costs are approximately 25% lower, but at a value of 0.5 M/kWe the inaccuracies in the data may become significant.

What is important to see from this study is that a fusion-fission machine may be economically competitive with pure fission devices in the future. The results of this study may be stated as follows: 1) liquid-metal coolants will be supremely difficult to use, 2) prohibitive temperatures found in small-radius vacuum walls re-enforce our opinion that large vacuum systems must be used, and 3) steady-state or pulsed devices with large vacuum systems surrounded by a Uranium bearing salt will be competitive in the future if the assumptions are valid.

Further studies of all energy losses and gains must be made. Especially important in large devices are the coolant pumping requirements. Schemes for efficiently utilizing the exhaust energy in pulsed devices must be brought to mind in the development of any pulsed systems. Finally, schemes to incorporate a fusion "core" with a "fission breeder blanket" must be advanced. Inclusion of solid-fuel elements in the blanket may be the next step in advancing the blanket design.

N. D. Woodson

References

1. F. Ribe, "Feasibility Study of a Pulsed Thermonuclear Reactor," LASL, LA-3294-MS.
2. S. O. Dean, "Heating of Vacuum Wall by Bremsstrahlung Radiation in a Pulsed Thermonuclear Reactor," USAEC Division of Research, 1965 (unpublished).
3. H. S. Carslaw and J. C. Jaeger, Conduction of Heat in Solids (Clarendon Press, Oxford, 1948).

2. ANALYSIS OF THE OPERATION OF A LONG ARC COLUMN

A long arc column generated by a hollow-cathode discharge has been operated over a broad range of parameters. In the study of various oscillation phenomena associated with the plasma having the arc as a source, it is important tto have a quantitative understanding of the conditions in the arc. For the analysis, we consider the geometry shown in Fig. X-29. We shall be concerned with the arc in the region between the baffle and

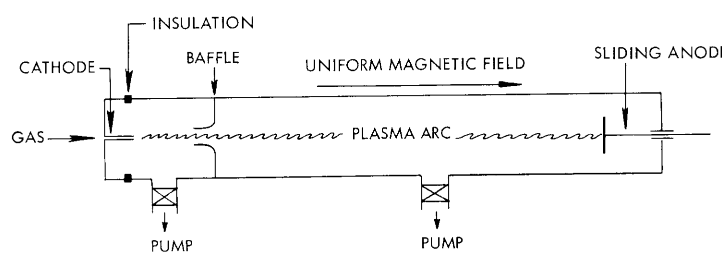

Fig. X-29. Geometry of the experiment.

the movable anode. Because of the differential pumping scheme, the plasma in this region is fully ionized, and a strong uniform magnetic field is applied along the axis of the column so that $\omega_i\tau_i > 1$ and $\omega_e\tau_e > 1$. In this case we need only be concerned with transport along the magnetic field lines. The transport equations for a steady-state fully ionized plasma may be written

$$\frac{d}{dz}\Gamma_e = 0 \tag{1}$$

$$\frac{d}{dz}\Gamma_i = 0 \tag{2}$$

$$m\Gamma_e \frac{d}{dz}\frac{\Gamma_e}{n} + \frac{d}{dz} nT_e = -enE - .51\frac{m_e}{\tau_e}(\Gamma_e - \Gamma_i) - .71\, n\frac{dT_e}{dz} \tag{3}$$

$$m_i\Gamma_i \frac{d}{dz}\frac{\Gamma_i}{n} + \frac{d}{dz} nT_i = enE + .51\frac{m_e}{\tau_e}(\Gamma_e - \Gamma_i) + .71\, n\frac{dT_e}{dz} \tag{4}$$

$$\frac{3}{2}\Gamma_e \frac{d}{dz} T_e + nT_e \frac{d}{dz}\frac{\Gamma_e}{n} = .51\frac{m_e}{n\tau_e}(\Gamma_e - \Gamma_i)^2 - 3\frac{m_e}{m_i}\frac{n}{\tau_e}(T_e - T_i) \tag{5}$$

$$\frac{3}{2}\Gamma_i \frac{d}{dz} T_i + nT_i \frac{d}{dz}\frac{\Gamma_i}{n} = 3\frac{m_e}{m_i}\frac{n}{\tau_e}(T_e - T_i), \tag{6}$$

where

$$\tau_e = \frac{(32)(2\pi)^{1/2}\,\epsilon_o^2 m_e^{1/2} T_e^{3/2}}{e^4\, n \ln \Lambda} \tag{7}$$

is the electron collision time. We have ignored the thermal conductivity in Eqs. 5 and 6, since the temperature gradient is generally small.

It is convenient to discuss this set of equations with variables expressed in dimensionless form. Hence we define

$$\Gamma_e = \frac{\Gamma_e}{n_o}\left(\frac{m_e}{T_{eo}}\right)^{1/2}, \quad \Gamma_i = \frac{\Gamma_i}{n_o}\left(\frac{m_e}{T_{eo}}\right)^{1/2}, \quad T_e = \frac{T_e}{T_{eo}}, \quad T_i = \frac{T_i}{T_{io}}$$

$$n = \frac{n}{n_o}, \quad m = \frac{m_i}{m_e}, \quad \theta = \frac{T_{eo}^2\epsilon_o^2}{e^4 n_o L \ln\Lambda}, \quad z = \frac{z}{L},$$

where n_o and T_{eo} are the density and electron temperature at some convenient reference point in the system, and L is the length of the plasma column.

From the momentum equations we obtain

$$\left[T_e + T_i - \frac{\Gamma_e^2 + m\Gamma_i^2}{n^2}\right]\frac{dn}{dz} + n\left[\frac{dT_e}{dz} + \frac{dT_i}{dz}\right] = 0 \tag{8}$$

which integrates to express the conservation of energy of the system:

$$\frac{\Gamma_e^2 + m\Gamma_i^2}{n} + n(T_e + T_i) = P = \text{constant}. \tag{9}$$

Making use of the energy equations, we obtain

$$\frac{dn}{dz} = (.015)\,\frac{(\Gamma_e-\Gamma_i)n^4}{P\theta m\Gamma_e\Gamma_i T_e^{1/2}}\,\frac{\left[\dfrac{.51m(\Gamma_e-\Gamma_i)\,\Gamma_i}{3n^2T_e}+1\right]}{\left[\dfrac{8\left(\Gamma_e^2+m\Gamma_i^2\right)}{5Pn}-1\right]} \tag{10}$$

$$\frac{dT_e}{dz} = \frac{2}{3}\,\frac{T_e}{n}\,\frac{dn}{dz} + \frac{.025}{\Gamma_e m\theta}\left[\frac{.51m(\Gamma_e-\Gamma_i)^2}{3n^2T_e}-1\right]\frac{n^2}{T_e^{1/2}} \tag{11}$$

$$\frac{dT_i}{dz} = \frac{2}{3}\,\frac{T_i}{n}\,\frac{dn}{dz} + .025\,\frac{n^2}{\Gamma_i m\theta T_e^{1/2}}. \tag{12}$$

Equations 10, 11, and 12 are the equations of interest. From these equations it is clear that the electron temperature may be adjusted by the balance of three processes: expansion cooling, Joule heating, and energy transfer caused by collision between electrons and ions. For the ions, since Joule heating from collision with electrons is of order $1/m$, only the first and third processes are effective. In the geometry under consideration, Γ_e is always positive. The sign of Γ_i is determined by whether or not an ion source is supplied at the anode, and this also determines the sense of the density gradient.

If we divide Eqs. 11 and 12 by (10), we obtain

$$\frac{dT_e}{dn} = \frac{2}{3}\,\frac{T_e}{n} + \frac{5P\Gamma_i\left[\dfrac{8\left(\Gamma_e^2+m\Gamma_i^2\right)}{5Pn}-1\right]\left[\dfrac{.51m(\Gamma_e-\Gamma_i)^2}{3n^2T_e}-1\right]}{3(\Gamma_e-\Gamma_i)\,n^2\left[\dfrac{.51m(\Gamma_e-\Gamma_i)\,\Gamma_i}{3n^2T_e}+1\right]}. \tag{13}$$

$$\frac{dT_i}{dn} = \frac{2}{3}\,\frac{T_i}{n} + \frac{5P\Gamma_e\left[\dfrac{8\left(\Gamma_e^2+m\Gamma_i^2\right)}{5Pn}-1\right]}{3(\Gamma_e-\Gamma_i)\,n^2\left[\dfrac{.51m(\Gamma_e-\Gamma_i)\,\Gamma_i}{3n^2T_e}+1\right]}. \tag{14}$$

The behavior of Eqs. 13 and 14 can be grouped naturally into three regimes:

$$\text{(I)}\qquad 6nT_e \gg \frac{m(\Gamma_e-\Gamma_i)^2}{n} \gtrsim \frac{m(\Gamma_e-\Gamma_i)\,\Gamma_i}{n} \tag{15}$$

$$\text{(II)} \qquad \frac{m(\Gamma_e-\Gamma_i)^2}{n} > 6nT_e > \frac{m(\Gamma_e-\Gamma_i)\,\Gamma_i}{n} \tag{16}$$

$$\text{(III)} \qquad \frac{m(\Gamma_e-\Gamma_i)^2}{n} \gtrsim \frac{m(\Gamma_e-\Gamma_i)\,\Gamma_i}{n} \gg 6nT_e \tag{17}$$

which express the various possible partitions of energy of the system.

In each case, Eqs. 13 and 14 reduce to a form that can be integrated exactly.

Case I

For the condition expressed by inequality (15), we obtain

$$T_e = (1+a)n^{2/3} - \frac{a}{n}, \tag{18}$$

where

$$a = \frac{\Gamma_i}{\Gamma_e - \Gamma_i}.$$

The behavior of (18) is shown in Fig. X-30, with the lower bounds for which (15) is valid shown in dotted lines. Since, in general $|\Gamma_i| \leqslant |\Gamma_e|$, therefore $\sim 1 \leqslant a \leqslant -0.5$ and for

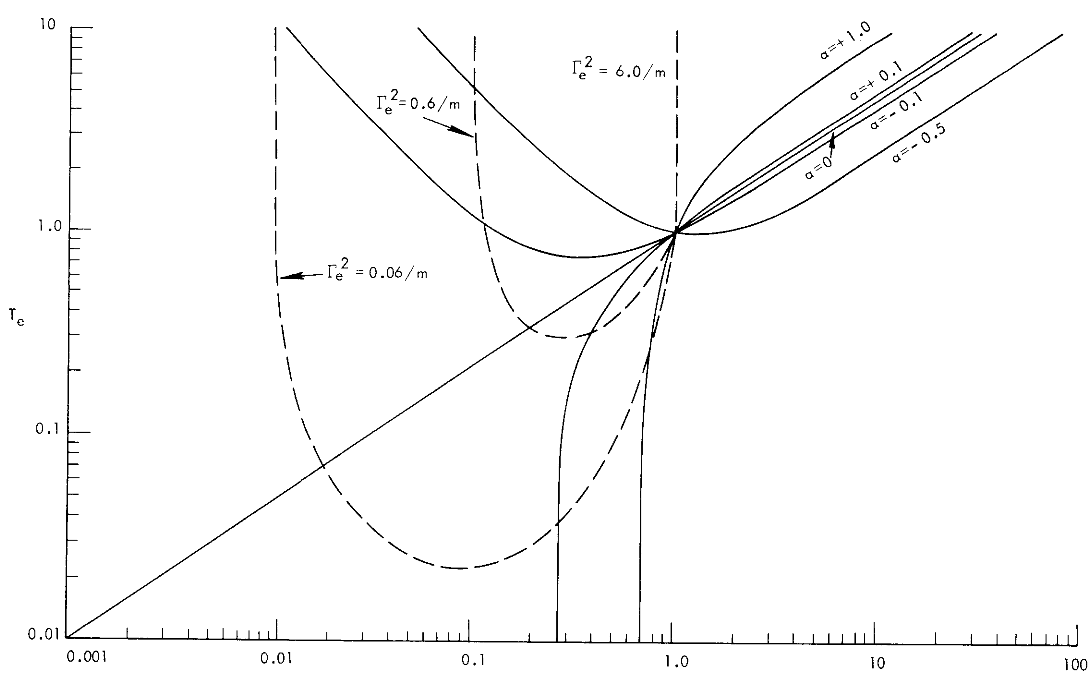

Fig. X-30. Regimes for Case I.

$n > 1$, we can express Eq. 18 by

$$T_e = n^{\delta} \tag{19}$$

$$1 \leqslant \delta \leqslant 0.$$

Case II

In case that inequality (16) is valid, we obtain from Eq. 13

$$T_e^2 = \left\{1 - .13m\Gamma_i(\Gamma_e-\Gamma_i)\left[1 - 1.3\,\frac{\left(\Gamma_e^2+m\Gamma_i\right)^2}{p}\right]\right\}n^{4/3}$$

$$+ .13\,\frac{m\Gamma_i(\Gamma_e-\Gamma_i)}{n}\left[\frac{1}{n^2} - 1.3\,\frac{\left(\Gamma_e^2+m\Gamma_i\right)^2}{pn^3}\right]. \tag{20}$$

For $n > 1$, the plasma behaves very closely to the ideal law

$$T_e = n^{2/3}. \tag{21}$$

Case III

When the drift energy is very large compared with the electron thermal energy, inequality (17) is valid, and the Joule heating effect is all-important. In this case

$$T_e = n^{2/3} + p\left[\frac{\Gamma_e^2 + m\Gamma_i^2}{Pn^2} - \frac{1}{n}\right]. \tag{22}$$

Here $P \gg 1$ and the second term is always dominant. If the temperature is not to rise rapidly down stream, the density must remain approximately constant for all practical purposes.

Having obtained the relationship between T_e and n, we can obtain the spatial variations of n, T_e, and T_i by integrating Eqs. 10, 11, and 12 in each case. The results are summarized in Table X-1.

From the results it is seen that the conditions of the arc are determined by the partition of the total energy that can be controlled by proper adjustment of the boundary conditions. In each case the behavior of the arc column along its length is characterized by the dimensionless parameter

Table X-1. Results of calculations.

$P = n(T_e+T_i) + \frac{(\Gamma_e^2+\Gamma_i^2)}{n}$

$P \approx n_oT_{eo} = 1$

If $\Gamma_i > 0$

$$n = \left\{1 - \left(3-\frac{\delta}{2}\right)(0.015)\frac{(\Gamma_e-\Gamma_i)}{\theta m\Gamma_e\Gamma_i}(1-z)\right\}^{-\frac{2}{6-\delta}};\quad T_i - T_{io} = \frac{5\delta}{2}\frac{\Gamma_e}{(\Gamma_e-\Gamma_i)}\left\{\left[1-(0.01)\frac{6-\delta}{2\delta}\frac{(\Gamma_e-\Gamma_i)}{\theta m\Gamma_e\Gamma_i}(1-z)\right]^{\frac{2}{6-\delta}} - \left[1-(0.01)\frac{6-\delta}{2\delta}\frac{(\Gamma_e-\Gamma_i)}{\theta m\Gamma_e\Gamma_i}\right]^{\frac{2}{6-\delta}}\right\}$$

$$n = \left\{1 + \left(3-\frac{\delta}{2}\right)(0.015)\frac{(\Gamma_e-\Gamma_i)}{\theta m\Gamma_e\Gamma_i}z\right\}^{-\frac{2}{6-\delta}};\quad T_i - T_{io} = \frac{5\delta}{2}\frac{\Gamma_e}{(\Gamma_e-\Gamma_i)}\left\{\left[1-(0.01)\frac{6-\delta}{2\delta}\frac{(\Gamma_e-\Gamma_i)}{\theta m\Gamma_e\Gamma_i}(1-z)\right]^{\frac{2}{6-\delta}} - 1\right\}$$

If $\Gamma_i < 0$

$$\Downarrow \left(\delta \to \frac{2}{3}\right)$$

- $|\alpha| \approx 1$ — collisional cooling

$$T_e = \left\{1-(0.025)\frac{(4-3\delta)}{2\delta}\frac{1}{\Gamma_e m\theta}(1-z)\right\}^{-\frac{2\delta}{4-3\delta}}$$

$$T_e = \left\{1+(0.025)\frac{(4-3\delta)}{2\delta}\frac{1}{\Gamma_e m\theta}z\right\}^{-\frac{2\delta}{4-3\delta}}$$

- $|\alpha| < 1$ — expansion cooling

$$T_e = \left\{1-(0.01)\frac{(6-\delta)}{2\delta}\frac{(\Gamma_e-\Gamma_i)}{\theta m\Gamma_e\Gamma_i}(1-z)\right\}^{-\frac{2\delta}{6-\delta}}$$

$$T_e = \left\{1+(0.01)\frac{(6-\delta)}{2\delta}\frac{(\Gamma_e-\Gamma_i)}{\theta m\Gamma_e\Gamma_i}z\right\}^{-\frac{2\delta}{6-\delta}}$$

$$\Downarrow \left(\text{as } \delta \to \frac{2}{3},\ P \approx 1\right)$$

$P \approx nT_e + \frac{\Gamma_e^2}{n} \geq 1$

$P \approx n_oT_{eo} \approx 1$

$$n = \left[1-\frac{0.04}{P\theta m\Gamma_e\Gamma_i}(1-z)\right]^{-3/8};\quad T_i - T_{io} = \frac{5P\Gamma_e}{3(\Gamma_e-\Gamma_i)}\left\{\left[1-0.04\frac{(\Gamma_e-\Gamma_i)}{P\theta m\Gamma_e\Gamma_i}(1-z)\right]^{3/8} - \left[1-0.04\frac{(\Gamma_e-\Gamma_i)}{P\theta m\Gamma_e\Gamma_i}\right]^{3/8}\right\}$$

$$n = \left[1+\frac{0.04}{P\theta m\Gamma_e\Gamma_i}z\right]^{-3/8};\quad T_i - T_{io} = \frac{5P\Gamma_e}{3(\Gamma_e-\Gamma_i)}\left\{\left[1+0.04\frac{(\Gamma_e-\Gamma_i)}{P\theta m\Gamma_e\Gamma_i}(1-z)\right]^{3/8} - 1\right\}$$

- $|\alpha| < 1$ — expansion cooling

$$T_e = \left[1-0.04\frac{(\Gamma_e-\Gamma_i)}{P\theta m\Gamma_e\Gamma_i}(1-z)\right]^{-1/4}$$

$$T_e = \left[1+0.04\frac{(\Gamma_e-\Gamma_i)}{P\theta m\Gamma_e\Gamma_i}z\right]^{-1/4}$$

- $|\alpha| \approx 1$

$P \approx \frac{\Gamma_e^2}{n} > 1$

$$n = \left[1-\frac{0.0256(\Gamma_e-\Gamma_i)}{\left(\Gamma_e^2+m\Gamma_i^2\right)\theta m\Gamma_e\Gamma_i}z\right]^{-3/11};\quad T_i - T_{io} = \frac{5\Gamma_e}{4m\Gamma_i(\Gamma_e-\Gamma_i)^2}\left\{\left[1+0.01\frac{(\Gamma_e-\Gamma_i)^2}{\theta\Gamma_e}z\right]^2 - 1\right\}$$

$$n = \left[1+\frac{0.0256(\Gamma_e-\Gamma_i)}{\left(\Gamma_e^2+m\Gamma_i^2\right)\theta m\Gamma_e\Gamma_i}(1-z)\right]^{-3/11};\quad T_i - T_{io} = \frac{5\Gamma_e}{4m\Gamma_i(\Gamma_e-\Gamma_i)^2}\left\{\left[1-0.01\frac{(\Gamma_e-\Gamma_i)^2}{\theta\Gamma_e}(1-z)\right]^2 - \left[1-0.01\frac{(\Gamma_e-\Gamma_i)^2}{\theta\Gamma_e}\right]^2\right\}$$

$$\Downarrow (\text{as } P \gg 1)$$

$P \approx \frac{\Gamma_e^2}{n} > 1$

$$n \approx n_o \qquad T_i - T_{io} = \frac{1.88}{m\Gamma_i(\Gamma_e-\Gamma_i)^2}\left\{\left[(0.0106)\frac{(\Gamma_e-\Gamma_i)^2}{\Gamma_e\theta}z+1\right]^{4/5} - 1\right\};$$

joule heating

$$T_e = \left[1-0.010\frac{(\Gamma_e-\Gamma_i)}{\Gamma_e\theta}(1-z)\right]^{2/5}$$

$$T_e = \left[1+0.010\frac{(\Gamma_e-\Gamma_i)}{\Gamma_e\theta}z\right]^{2/5}$$

$$\theta = \frac{T_{eo}^2 \epsilon_o^2}{e^4 n_o L \ln \Lambda}$$

which, together with the electron and ion fluxes Γ_e and Γ_i, completely specifies the system.

J. C. Woo

3. TRANSVERSE DIFFUSION OF A LONG PLASMA COLUMN

The diffusion of a magnetically confined plasma across the field lines has been considered by many authors. Simon[1] has pointed out that for an open system the transverse diffusion is coupled to the longitudinal electron mobility; consequently, the diffusion rate is considerably greater than the unidirectional ambipolar rate. In his analysis, Simon assumes that $E_R/E_L \approx L/R$, and for a stubby apparatus such as the experiment of Neidigh, to which Simon's analysis was directed, the radial electric field may be neglected. In a long plasma column, for example, in many recent arc experiments, $L/R \gtrsim 10$, and the radial electric field is significantly larger than the longitudinal field. The fact that a large radial electric field can exist suggests that the Simon short-circuiting effect is not fully effective. The longitudinal mobility is, however, much greater than any transverse loss mechanism for the electrons; consequently, the radial electric field will seek for itself a value that is consistent with the longitudinal mobility of the electrons and limits the transverse diffusion of the ions. The resulting loss rate will lie between the ambipolar and the Simon short-circuit process rates.

We shall evaluate the effect of the presence of a radial electric field, using a simple diffusion model. As is typical of arc plasmas, both the density and the electron temperature have approximately the same radial profile; consequently, the assumption that the diffusion and mobility coefficients are constant in space is not too bad an approximation.

Writing the continuity equation for the electrons and single charged ions, we have

$$\frac{\partial n_e}{\partial t} = D_e \frac{\partial^2 n_e}{\partial x^2} - b_e \frac{\partial}{\partial x}\left(n_e \frac{\partial \phi}{\partial x}\right) + D_e \frac{\partial^2 n_e}{\partial z^2} - b_e \frac{\partial}{\partial z}\left(n_e \frac{\partial \phi}{\partial z}\right) \tag{1}$$

$$\frac{\partial n_i}{\partial t} = D_i \frac{\partial^2 n_i}{\partial x^2} + b_i \frac{\partial}{\partial x}\left(n_i \frac{\partial \phi}{\partial x}\right) + D_i \frac{\partial^2 n_i}{\partial z^2} + b_i \frac{\partial}{\partial z}\left(n_i \frac{\partial \phi}{\partial z}\right). \tag{2}$$

Here we have used a rectangular coordinate system with the magnetic field in the z-direction. Even though we are specifically interested in the space charge that would exist across the field lines, the net imbalance between the electron and ion, nevertheless, is small, and we can still set $n_e = n_i = n$.

Eliminating the transverse mobility between the two equations, we obtain

$$\frac{\partial n}{\partial t} = D_\perp \frac{\partial^2 n}{\partial x^2} + D \frac{\partial^2 n}{\partial z^2} - b\left(\frac{\partial n}{\partial z}\frac{\partial \phi}{\partial z} + n \frac{\partial^2 \phi}{\partial z^2}\right), \tag{3}$$

where

$$D_\perp = \frac{D_{e\perp} b_{i\perp} + D_{i\perp} b_{e\perp}}{b_{i\perp} + b_{e\perp}} \approx \frac{D_i}{b_i} b_{e\perp} + D_{e\perp} \tag{4}$$

$$D = \frac{D_e b_{i\perp} + D_i b_{e\perp}}{b_{i\perp} + b_{e\perp}} \approx D_e \tag{5}$$

$$b = \frac{b_e b_{i\perp} + b_i b_{e\perp}}{b_{i\perp} + b_{e\perp}} \approx b_e. \tag{6}$$

Since the longitudinal electron mobility is high, space charge cannot exist in the axial direction. For a long column, we can assume $\partial^2\phi/\partial z^2 \approx 0$, and $\partial\phi/\partial z = -E_z$ = constant.

Assuming that a plasma source exists only along the axis $x = 0$, away from the source, Eq. 3 is homogenous:

$$D_\perp \frac{\partial^2 n}{\partial x^2} + D \frac{\partial^2 n}{\partial z^2} + bE_z \frac{\partial n}{\partial z} = 0 \tag{7}$$

$$n = \frac{N_o}{\left[1 - \exp\left(-\frac{x_o}{p}\right)\right]} \left[\exp\left(-\frac{1}{2}\frac{x}{p}\right) - \exp\left(-\frac{1}{2}\frac{(2x_o - x)}{p}\right)\right] \cdot \left[\exp\left(-\frac{z}{q}\right)\right] \cos\frac{\pi}{L} z, \tag{8}$$

where

$$p = \sqrt{\frac{D_\perp}{D}} \frac{1}{\left(\frac{b^2 E_z^2}{D^2} + \frac{\pi^2}{L^2}\right)^{1/2}} \tag{9}$$

$$q = \frac{D}{bE_z}. \tag{10}$$

The axial density distribution is plotted in Fig. X-31 for a range of values of q. Making use of the Einstein relation yields

$$q \approx \frac{T_e L}{q\phi_o}.$$

In the external plasma of the hollow cathode arc

$$\frac{L}{2} \gtrsim q \gtrsim \frac{L}{5},$$

and this profile is in good agreement with the experimental observation as shown in Fig. X-31. The slight disagreement at the ends is due to the existence of a sheath, and

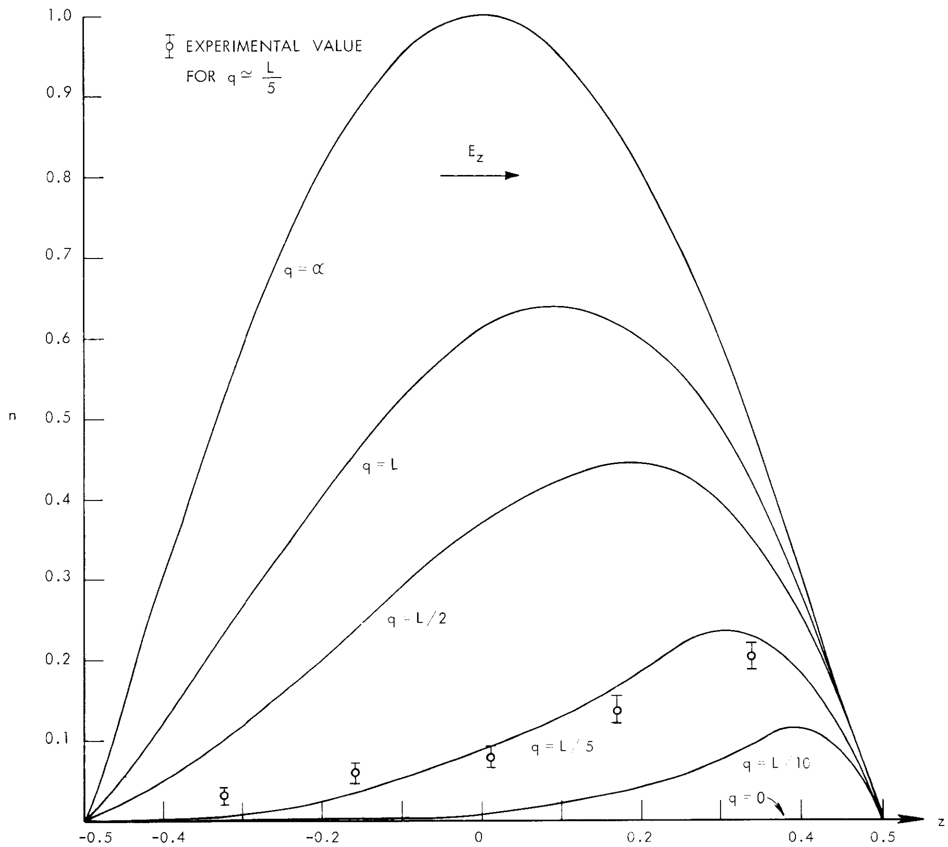

Fig. X-31. Axial density distribution for a range of values of q.

therefore the density of the interior plasma does not vanish at the boundary.

The radial e-folding distance is now given by

$$2p = 2\sqrt{\frac{D_\perp}{D}}\,\frac{1}{\left(\dfrac{b^2E_z^2}{D^2}+\dfrac{\pi^2}{L^2}\right)^{1/2}} \approx 2\left(\frac{T_i}{T_e}\right)^{1/2}\frac{1}{a_e}\,\frac{L}{\pi},$$

where $a_e = \omega_e\tau_e$.

This result differs from Simon's in that the e-folding distance is inversely proportional to α_e rather than α_i and, for the condition of the arc, leads to a value of the order of centimeters which is also consistent with observation (rather than a fraction of a meter as expected from the Simon result).

The question arises as to the effect of the large-scale fluctuations arising from drift-wave instabilities that could lead to turbulent diffusion. These oscillations generally appear in the kilocycle range. Since the electron mobility determines the over-all diffusion rate of the system, and the electrons traverse the system in microseconds, these oscillations cannot significantly affect the loss rate of the plasma in an open system of moderate length.

J. C. Woo

References

1. A. Simon, Report P/366, Second International Conference on the Peaceful Uses of Atomic Energy, Geneva, 1958.